Chapter 7

Simulated ENSO Sensitivity to Climate

Knock on the sky and listen to the sound.

Zen saying

This chapter examines the sensitivity of tropical Pacific interannual variability to changes in the climatological background state. Chapter 5 showed that although a wide variety of climate perturbations can affect the equatorial Pacific, the equatorial structure of the response tends to be similar in each case. Due to strong coupled feedbacks like those active in ENSO, the Pacific climatology generally responds with either an El Niño-like warming (with a weakened zonal SST gradient, relaxed trades, relaxed currents, and a flatter thermocline) or a La Niña-like cooling (with a sharper zonal SST gradient, stronger trades, stronger currents, and a steeper thermocline slope).

This chapter therefore focuses primarily on the ENSO sensitivity to a single climate parameter, the strength of the equatorial zonal wind stress. Section 7.1 draws on the ideas of Chapter 6 to explain how the growth of small disturbances is affected by the strength of the climatological equatorial trades, and investigates the extent to which the ENSO sensitivity to other climate parameters resembles the sensitivity to trade wind strength. Section 7.2 then considers how a change in the equatorial trades affects the transient ENSO response to strong wind events, and extends the climate sensitivity map to stronger values of the air-sea coupling. Section 7.3 discusses the effects of climate changes in the stochastic context, focusing on ENSO predictability and the extent to which observed ENSO changes can be detected and attributed to climate changes. Section 7.4 concludes with a climate sensitivity analysis of a hybrid coupled GCM.

7.1 Small-amplitude regime

How is the linear behavior of ENSO affected by a change in climate? In this section, we examine the stability of the tropical Pacific climatology to small perturbations, in

the absence of stochastic excitation. The results in this linear regime will prove relevant not only to the growth of forecast errors, but also to the behavior of ENSO at realistic amplitudes.

7.1.1 Design of the experiments

To explore the sensitivity of a small-amplitude ENSO to climate changes, we perform a suite of experiments in the intermediate model. The plan is to impose a climate perturbation, spin up the model to its new climatology, kick the model with a transient disturbance and characterize the resulting variability. The initial background state of the anomaly model is prescribed from the control run climatology described in Section 4.2.4. For a prototype we consider first the effect of a change in the strength of the trade winds, by imposing an equatorial zonal stress perturbation of the form (5.1), which is constant in the zonal direction, and has a Gaussian shape in the meridional with a meridional halfwidth of 15° latitude and an equatorial maximum of $\widetilde{\overline{\tau}^*_x}$.

The first task is to spin up the model onto its new attractor. Experience suggests that the adjustment to the attractor is most rapid when the climate perturbation is phased in gradually instead of all at once. Thus we linearly increase the amplitude of the climate perturbation from zero to the value of interest over a period of 20 years (Stage I), after which the perturbation parameter is held constant. To attenuate any further effects of the adjustment, the model is run for another 30 years (Stage II) prior to collecting data.

The next task is to characterize the attractor prior to the disturbance. The model trajectory is recorded for 10 years (Stage III). Over the range of trade wind strengths in this experiment, the attractor is generally found to be either a stable fixed point or a very weak limit cycle. (We have observed no evidence of multiple or strange attractors at the standard coupling, though we have not mounted a systematic search.) Thus the attractor appears to be well-characterized by its time-mean state.

The final task is to ping the model with a transient disturbance and characterize the response (Stage IV). At the beginning of year 60 the model is subjected to a slight weakening of the trade winds as in Section 4.3.1, with a peak stress perturbation amplitude of $\tilde{\tau}^*_x = 0.02$ dPa for 3 months on the equator at 165°W. This perturbation is weak enough to keep the response fairly linear, but still strong enough to knock the trajectory far off of any weak limit cycle. The subsequent evolution of the model is recorded for 10 years, and the reference state from Stage III is subtracted to give a timeseries of anomalies. This brings the total model time required for each linear climate change experiment to 70 years.

Stages I–IV are then repeated at different values of the perturbation parameter, spanning the range of interest. For the prototype case this corresponds to 11 experiments with $\widetilde{\overline{\tau}^*_x}$ running from -0.1 dPa to 0.1 dPa at intervals of 0.02 dPa. Altogether, the total model time required for the sensitivity map is 770 years.

7.1.2 Overview of the equatorial-trades prototype

Equatorial SST anomalies

How does the evolution of small disturbances depend on the strength $\widetilde{\overline{\tau}^*_x}$ of the equatorial trades? Fig. 7.1 summarizes the response of SST anomalies to a small disturbance, for

different strengths of the climatological equatorial wind stress. The model SSTA generally evolves like a standing oscillation, though there is some westward propagation in the west and eastward propagation in the east. For strong mean trades (a), ENSO has a short period and the SST variability is focused near 140°W. In contrast, for weak mean trades (f), ENSO has a long period and is active farther east, with weak SST anomalies of opposite sign in the western Pacific. The ENSO mode is damped in nearly all of these regimes, but the damping rate varies with the trade wind strength: the oscillation is least damped when the trades are either very strong (a) or close to their normal strength (c), and are most damped when the trades are very weak (f) or only moderately strengthened (b).

Focusing on the first year after perturbation, it is evident that the short-term transients have a somewhat simpler dependence on the strength of the trades than do the modal properties. The initial warming is most intense when the trades are only slightly stronger than in the control (c), suggesting that the control run is nearly optimal for the initial growth of SSTA errors.

Heat budget phasors

What is responsible for these changes in ENSO behavior? The phasor diagrams in Fig. 7.1 show the relative roles of advection, surface heat fluxes, and mixing in the evolution of the SST anomalies. The phasor plots are derived as follows. At the longitude and time scale of peak equatorial SSTA variance, the differenced tendency terms are analyzed as a function of scale and time using a Morlet wavenumber-6 mother wavelet. The wavelet phase (relative to SSTA) and amplitude (relative surface heat flux) of each tendency term are computed, vector-averaged over the middle third of the timeseries, and then plotted together as a phasor in the diagram. The diagram reads like a clock, with the SSTA peak occurring at 3 o'clock: an arrow that points to the right is in phase with SSTA, and an arrow that points upward leads SSTA by 90°. The phasors are plotted in order of decreasing amplitude so that they do not hide each other. Processes with an amplitude less than 15% of the surface heat flux, i.e. inside the dotted circle, are not plotted but are accumulated in a residual phasor which is plotted only if it lies outside the dotted circle.

The phasors in the diagram are labeled in shorthand, with "m" denoting the background state of the control run (not the perturbed model climatology), and "p" denoting a perturbation from this background state. Thus changes in "uptm" ($-u'\partial_x\overline{T}$) isolate dynamical changes in the amplitude and phase of the zonal currents relative to SSTA, unconfounded by changes in mean SST. Similarly, "wmtp" ($-\overline{w}\partial_z T'$) isolates amplitude and phase changes in the anomalous vertical temperature structure, unconfounded by changes in mean upwelling. The additional effects of changes in the climatological fields, which result directly from the imposed zonal stress, are represented by terms such as "uptp" ($-u'\partial_x T'$). The total SSTA tendency ("tdot" or $\partial_t T$) is the vector sum of all of the individual tendency phasors.

Fig. 7.1 shows that the ENSO mechanism at the longitude of peak SSTA variability is greatly affected by a change in the strength of the trade winds. For the control case (d), the oscillation is almost entirely due to $-\overline{w}\partial_z T'$, which plays both destabilizing and transitioning roles. In this case the $-w'\partial_z\overline{T}$, $-\overline{v}\partial_y T'$, and $-u'\partial_x\overline{T}$ terms, while small, help to maintain the oscillation amplitude in the face of strong damping by the surface heat

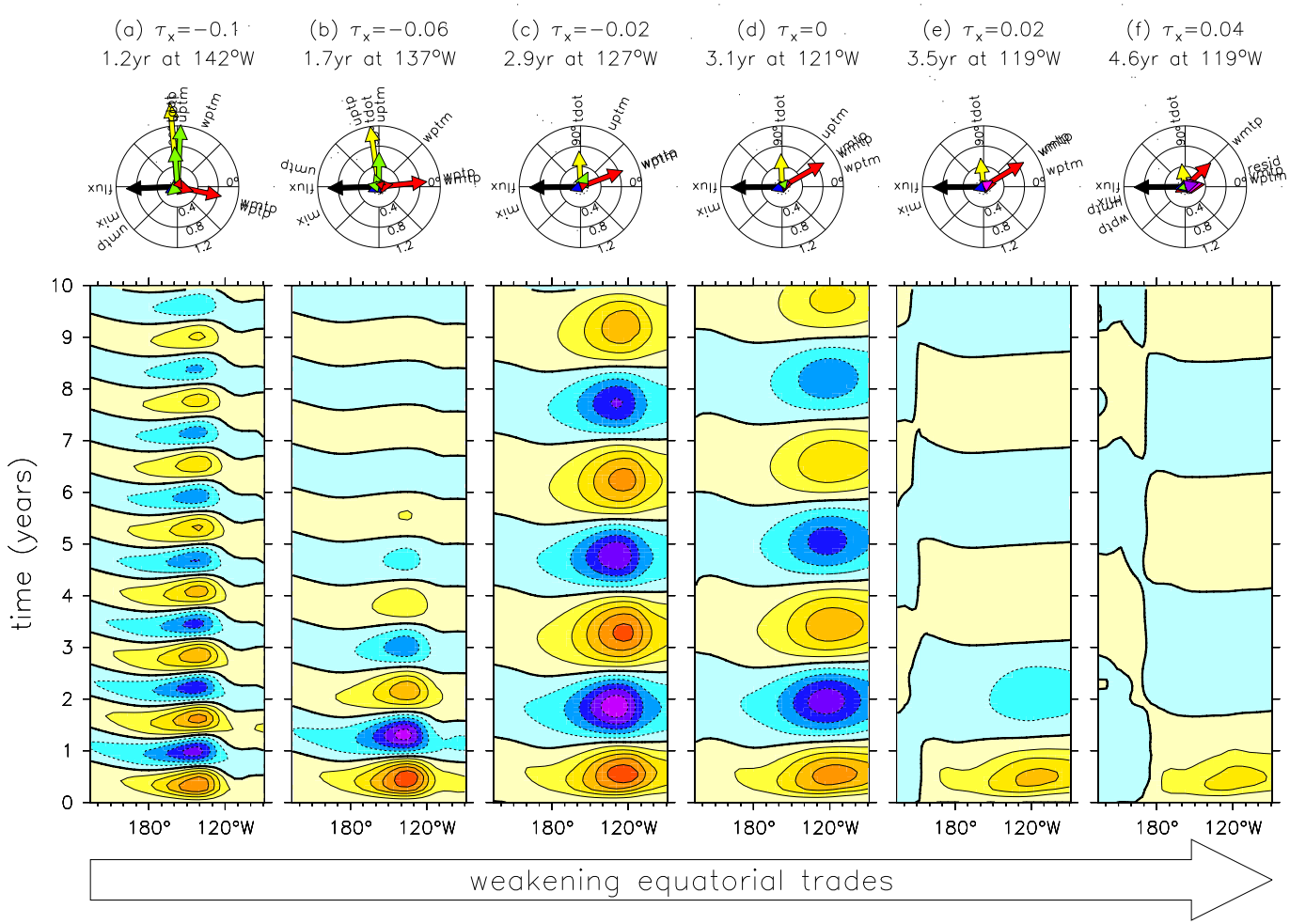

Figure 7.1: Change in ENSO due to a change in mean trade winds, as simulated by the noiseless intermediate model. Time-longitude plots (bottom row) show the equatorial (2°S–2°N) evolution of SST errors induced by a weak westerly wind burst in the central Pacific at the start of year 0. The errors are small (contour interval is 0.1°C) and so the dynamics are nearly linear. Labels at top indicate the amplitude of the imposed climate perturbation (trades weaken to the right), the oscillation period, and the longitude of peak variance. Phasors (middle row) show the amplitude (relative to surface heat flux) and phase lead (relative to local SSTA) of the temperature tendency terms in the equatorial band at the longitude of peak variance.

flux and weak dissipation by horizontal mixing.

As the trades strengthen, $-\overline{w}\partial_z T'$ comes more and more into phase with SSTA, eventually becoming a pure destabilizer. The destabilizing effect of $-\overline{w}\partial_z T'$ is also enhanced by stronger mean upwelling associated with the intensified trades. It is now *zonal* advection that plays the role of the "transitioner," the inertia that carries the system past the climatological equilibrium. The increased zonal advection is largely due to the strengthening of the equatorial zonal current anomalies, but there is also a contribution from the steeper $\partial_x \overline{T}$ which increases the SST sensitivity to the zonal currents.

As the trades weaken, on the other hand, the deepening of the climatological thermocline in the east and the reduction of in equatorial upwelling decrease the SST sensitivity to thermocline motions. This weakening of $-\overline{w}\partial_z T'$ leads to an increase in both the oscillation period and the damping rate of ENSO. The growth effect of this term is further weakened by the increase in the phase lead of $-\overline{w}\partial_z T'$ ahead of SSTA. For very weak trades, equatorial upwelling in the east disappears. At this point, the only thermal connection between surface and subsurface is south of the equator, associated with upwelling induced by the cross-equatorial southerlies. This meridional asymmetry leads to an increased role for meridional advection as a destabilizing term at the equator. The $-w'\partial_z \overline{T}$ term also enters as a destabilizer, as the eastward shift of the statistical stress response brings stronger upwelling variations into the east Pacific region of strong $\partial_z \overline{T}$.

Linear evolution of forecast errors

Given these results, what can we say about how small errors might evolve in a forecast situation? Fig. 7.1 can be interpreted in terms of the evolution of small SST forecast errors, arising from an unanticipated westerly wind burst in the western Pacific. For weak stochastic forcing, a succession of easterly and westerly bursts would result in a linear superposition of the responses shown in Fig. 7.1.

On the basis of this figure one can then say several things about predictability in the linear context. First, errors will tend to grow more rapidly (during the first 1–3 months after the disturbance) when the climatological trades are strong than when they are weak. Second, the saturated error is likely to be greatest when the trades are just slightly stronger than in the control run, since this case has both the strongest peak error value (which occurs around month 7) and also the strongest sustained error amplitude; interestingly, empirical analysis of *observed* SSTAs (Penland and Sardeshmukh, 1995) suggests that the maximum error growth due to modal interference does indeed tend to peak at around 7 months lead. Third, the errors will tend to lie farther west when the climatological trades are strong than when they are weak. And finally, for episodic stochastic forcing, one can expect a "return of predictability" a year or so after a large wind burst, as the SSTA error crosses zero. The return time is simply half the oscillation period, and so increases as the climatological trades weaken.

7.1.3 Evolution of the equatorial vertical structure

What is going on below the surface to cause these changes in the mechanism and behavior of ENSO? In this section we examine vertical slices of the simulated equatorial

fields along the equator. This reveals how changes in the vertical thermal structure of the ocean, and in the zonal phasing of the stress anomalies, have a large impact on the oscillation amplitude and period.

Control run

Fig. 7.2 shows equatorial snapshots from the small-amplitude control run. The imposed westerly stress disturbance weakens equatorial upwelling and generates eastward equatorial current anomalies, associated with an eastward-moving equatorial Kelvin wave and a westward-moving off-equatorial Rossby wave pair. As the Kelvin wave propagates into the eastern Pacific, it deepens the local thermocline and induces a subsurface warming in the east. The mean upwelling $\overline{w}$ then conveys the subsurface signal into the mixed layer, especially in the central Pacific were $\overline{w}$ is strongest. The downwelling anomalies in the central Pacific contribute to the SST increase as less cold water is advected into the mixed layer. The result is a surface warming that is shifted $\sim 20^\circ$ west of the subsurface warming. The SST increase then gives rise to westerly stress anomalies, which peak $\sim 50^\circ$ west of the SSTA. These stress anomalies, in turn, further weaken the equatorial upwelling, strengthen the eastward currents, and enhance the deepening of the thermocline in the east to complete the feedback cycle and plunge the system into a warm event.

Note that as the El Niño is developing, the thermocline is gradually shoaling in the off-equatorial western Pacific. This shoaling is achieved by upwelling long Rossby wave signals, which radiate westward from the region of strong cyclonic curl on the poleward flanks of the westerly stress anomalies in the central basin. The discharge of heat content from the western off-equatorial Pacific gradually drains the equatorial band of heat content as well, as short Rossby waves convey mass poleward along the western boundary and induce upwelling Kelvin wave signals at the equator. The shoaling of the equatorial thermocline erodes the surface warming, which peaks about 7 months after perturbation. Following the peak, mass continues to drain out of the equatorial band, until the surface temperature, winds, and thermocline slope return to normal around month 14.

The system, however, is still out of balance. Note that at this point (1) the equatorial thermocline is everywhere shallower than normal, (2) the surface currents are westward all along the equator, and (3) the draining of heat content out of the equatorial band continues, due to the anomalously shallow thermocline in the off-equatorial western Pacific. Because the climatological thermocline is shallower in the east, the overall shoaling of the thermocline induces a greater cooling of T_e in the east than in the west. Entrainment on the zonally-asymmetric $\partial_z T'$ then generates an anomalous westward SST gradient, which produces easterly stress anomalies that further enhance the equatorial cooling.

The key point is that slow equatorial recharge/discharge processes, which produce a phase lead of the thermocline depth ahead of SSTA in the east Pacific, are central to the oscillation in the control case. Also important are the zonal current anomalies, which reverse in the central basin even before the winds disappear. By month 13, for example, easterly currents have developed at the equator despite the continued presence of westerly stress. These westward currents act on the climatological westward SST gradient to produce a cooling tendency in the central Pacific, which hastens the demise of the warm event.

Together, these factors cause the system to overshoot the climate equilibrium and sow

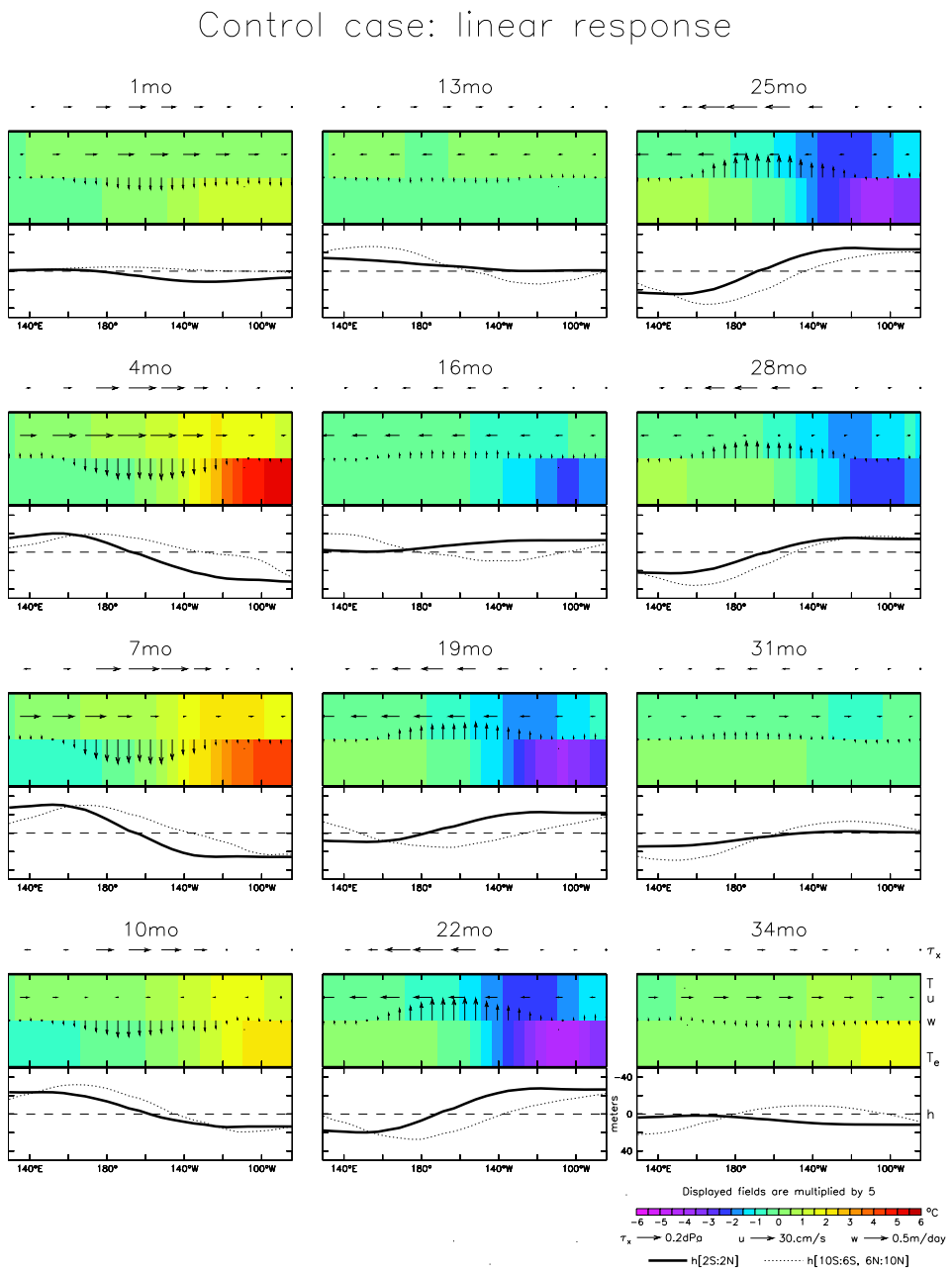

Figure 7.2: Equatorial snapshots at three-month intervals from the small-amplitude control case. Time flows down each column then left to right, and is indicated above each panel in terms of months since a weak westerly stress perturbation was imposed. Bottom right panel gives contour/vector keys for all panels. Vectors indicate anomalies of (top to bottom) zonal surface stress, mixed layer zonal current, and upwelling velocity at the mixed layer base. Shading indicates the anomalous temperature in the well-mixed surface layer (top) and at 50 m depth (bottom). Bottom subpanel shows the thermocline depth anomaly (ordinate reversed), at the equator (2°S–2°N, solid) and off-equator (6–10° N/S, dotted).

the seeds of a cold event, which develops rapidly as easterly winds amplify the thermocline slope, upwelling and easterly currents along the equator. Because the easterly winds are associated with anticyclonic curl off-equator, the western Pacific thermocline gradually deepens via downwelling Rossby signals and their reflection into downwelling Kelvin signals. By month 25 the western Pacific is recharged of heat content, and as this mass begins streaming into the equatorial band along the western boundary, the cold event reaches its peak. By month 34, the system has come full cycle and is poised to begin another El Niño.

In the off-equatorial thermocline, one can see a series of bumps and dips moving slowly westward with a wavelength slightly greater than the width of the Pacific, and a speed of roughly 0.25 m s^{-1}. One might be tempted to infer that coupled Rossby waves were somehow propagating coherently from the eastern to the western boundary, triggering equatorial changes by reflecting as Kelvin waves. As pointed out by Battisti (1989), however, the off-equatorial signal is more the *product* of the equatorial events than the cause of them. In particular, note that the amplitude of the off-equatorial anomaly weakens markedly as it moves into the central basin (during the transitions between ENSO events), and then strengthens again as it approaches the western boundary (as an ENSO event reaches its peak). The off-equatorial western Pacific thermocline signal arises more from ENSO-associated wind curl in the western/central basin than from coupled Rossby signals propagating in from the east. Rather than thinking of the ENSO period in the control run as being related to the time required for off-equatorial thermocline depth anomalies to propagate from the eastern boundary to the western boundary, it is better to think of the period as being set by the time required for the off-equatorial signal in the west (which is generated directly by ENSO stress curl) to reverse the equatorial zonal currents, erode the equatorial zonal-mean thermocline depth, and thereby feed back on the equatorial SST and off-equatorial stress curl.

Case with strong mean trades

How does a strengthening of the climatological trades alter this picture? Fig. 7.3 shows equatorial snapshots from the strong-trades case. As described in Section 7.1.2, the variability in this case has a shorter period and is shifted farther west than in the control run. One key difference in the structure of this mode is that despite substantial thermocline variability in the eastern Pacific, Fig. 7.2 indicates very little change in entrainment temperature along the South American coast. This is because the climatological thermocline is so shallow in the east that T_e is relatively insensitive to variations in h (see Fig. 4.7). In the real world, a desensitizing effect like this could arise due to a shoaling of the mixed layer depth as thermocline approaches the surface.

Such a change in the subsurface anomaly structure has a profound effect on the simulated ENSO. During the initial warming in the central basin, the separation of the SST anomalies from the coast gives rise to easterly stress anomalies in the far eastern Pacific. These easterlies generate anomalous upwelling, which acts on the strong $\partial_z T$ in the east and to further suppress warming there. As a result, there is hardly any warming in the east despite the anomalously deep thermocline. This opens the door for even stronger easterly stress anomalies in the east, and since the easterlies and associated upwelling are displaced slightly westward of the cold peak, they act to propagate the cold SSTA westward. By

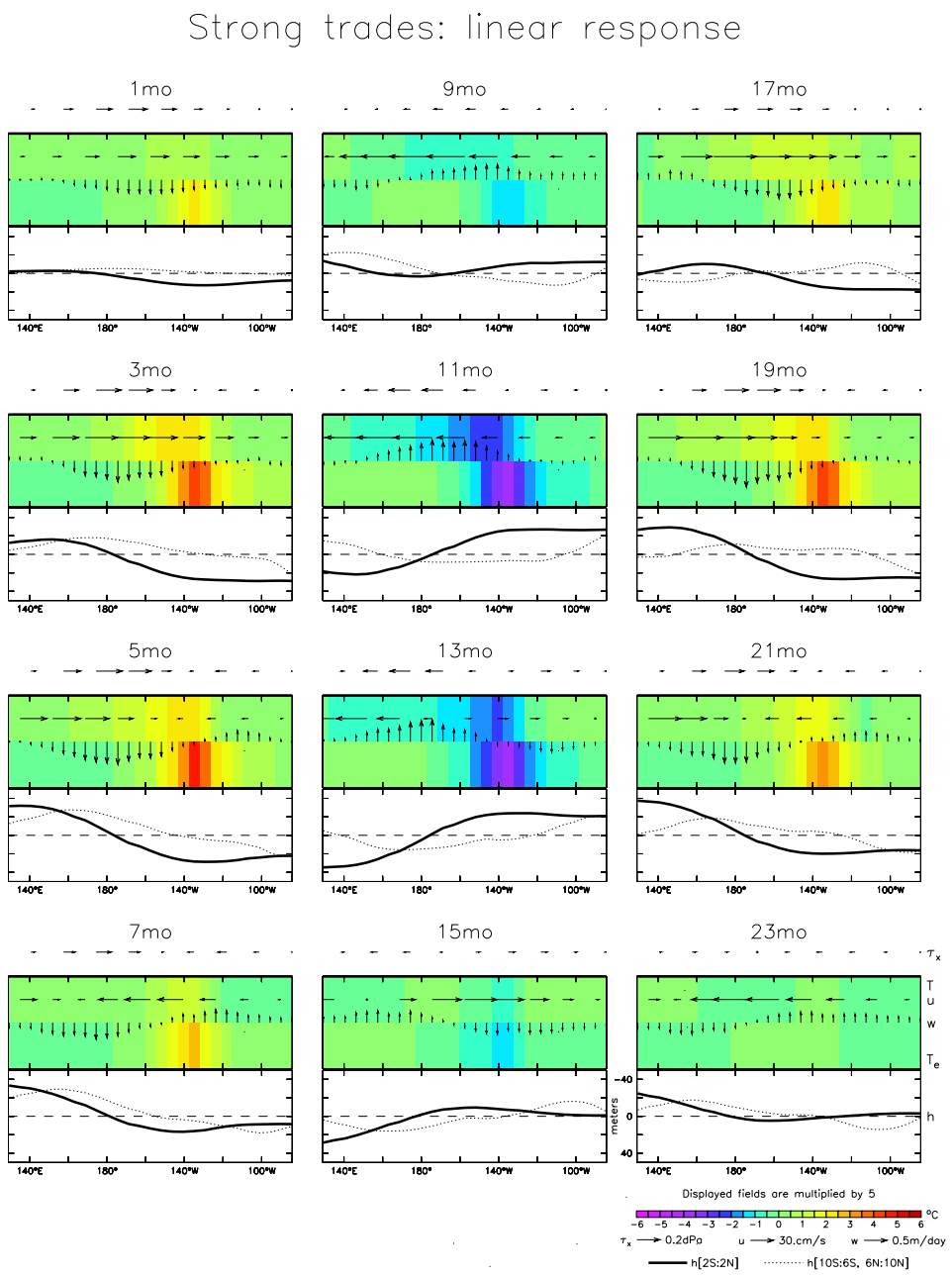

Figure 7.3: Equatorial snapshots at two-month intervals from the small-amplitude case with strengthened trades ($\widetilde{\overline{\tau}_x^*} = -0.1$ dPa). Otherwise as in Fig. 7.2.

month 9, the easterlies have propagated into the central Pacific to displace the westerly anomalies that had prevailed there, and the cycle then repeats with the opposite sign.

The model ENSO in this case thus resembles the so-called "SST mode," of the type described by Neelin (1991). The propagation of this mode depends on a competition between zonal/vertical advection by the anomalous currents, and vertical advection by mean upwelling acting on the anomalous thermocline. During the first few months after perturbation, the westerly current anomalies in the central Pacific are displaced to the west of the westerly stress anomalies, which are themselves displaced to the west of the surface warming. Since the zonal advective warming is displaced west of the SSTA, it tends to induce westward propagation of the modal structure. This propagation however, is opposed by upwelling on the anomalously deep thermocline, which induces a surface warming far to the east of westerly stress anomalies. Near 140°W, where $\partial_h T_e$ reaches its maximum, both processes are important and the SSTA does not propagate. Only where the thermocline effect is weak, such as in the western Pacific where the thermocline is very deep, and in the far eastern Pacific where T_e saturates, is westward propagation evident.

The meridional structure of the thermocline in this case undulates in a manner very similar to the control run, with warm water flowing off-equator during warm events and onto the equator during cold events. In contrast to the control run, however, these thermocline motions have a relatively small effect on the evolution of surface temperatures compared to zonal advection. The La Niña-like mean state, with its strong $\partial_x T$ in the central Pacific and saturated T_e in the eastern Pacific, naturally favors the zonal advective effect over the thermocline effect, and zonally-propagating mechanisms over meridional recharge/discharge mechanisms.

The amplitude of the oscillation is maintained by entrainment on in-phase thermocline depth anomalies near 140°W, which amplify SSTA near the peak of each cycle. The seed for localized feedbacks is planted by the development of SSTAs in the eastern Pacific which are of opposite sign to those in the central Pacific. The east Pacific SSTAs are induced by an atmospheric bridge, which generates upwelling anomalies that act on the strong $\partial_z T$ in the east. Rossby wave signals emanating from the eastern boundary, which are enhanced by the early wind reversal in the east, provide the delayed negative feedback essential for oscillation. The Rossby signals induce a strong westward-propagating reversal of the equatorial zonal current anomalies, which then act on the strong $\partial_x T$ to transition the system between warm and cold events. Because the timescale in this case is set by a resonant interaction involving zonal advection and eastern boundary reflections, it depends fundamentally on the speed of coupled Rossby waves.

Case with weak mean trades

What is the effect of a *weakening* of the climatological trades? Fig. 7.4 shows equatorial snapshots from the weak-trades case. In this case the westerly stress disturbance induces only a slight warming of the surface in the east. The climatological thermocline is so deep in the eastern Pacific that T_e is relatively insensitive to motions of the thermocline, and $\partial_x \overline{T}$ and $\partial_z \overline{T}$ are weakened so that zonal current and upwelling anomalies have less of an effect on SST. Thus the equatorial positive feedbacks are weak and the oscillation is rapidly damped. The off-equatorial Rossby signals, which are induced entirely by the coupled wind

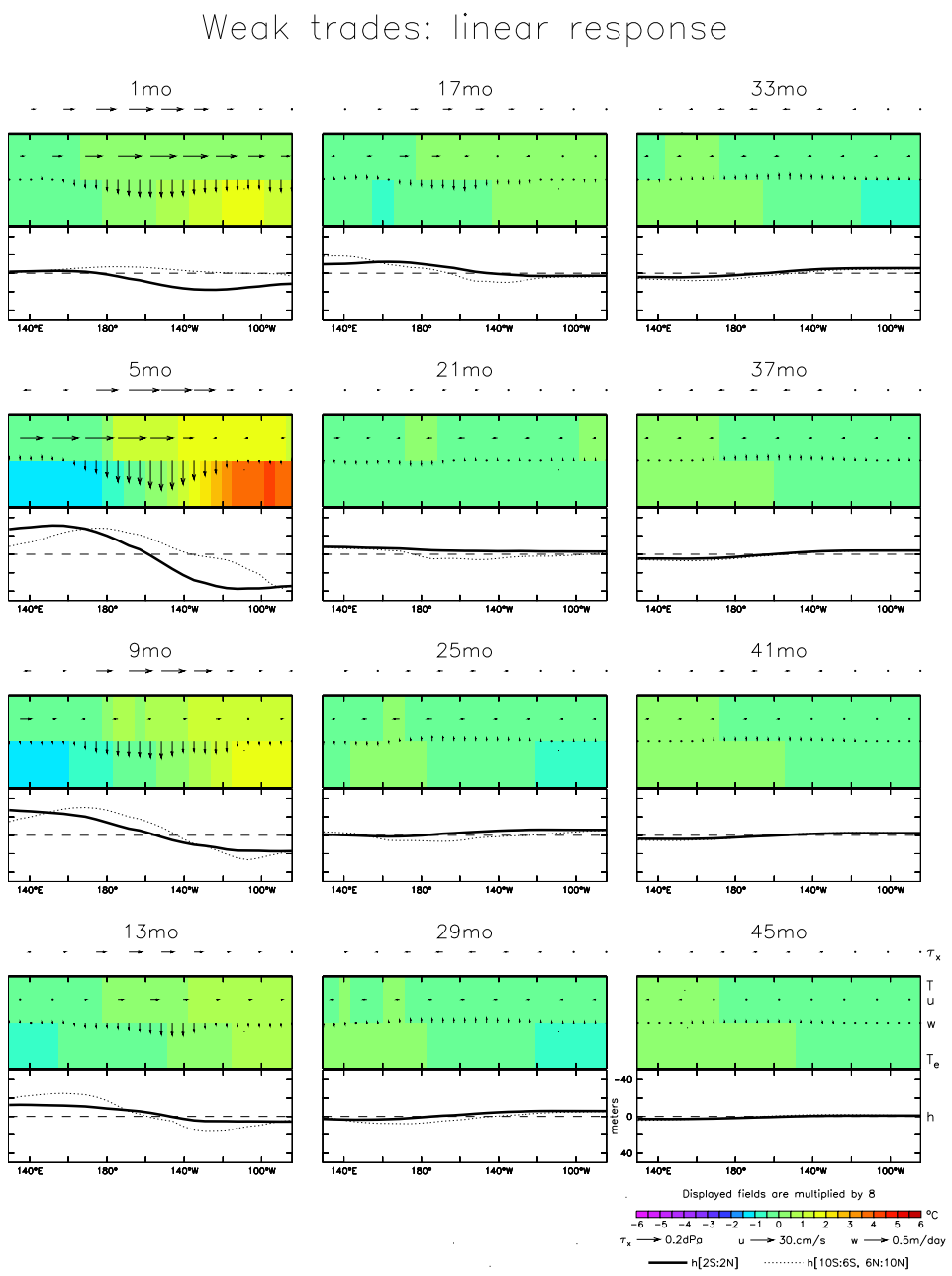

Figure 7.4: Equatorial snapshots at four-month intervals from the small-amplitude case with weakened trades ($\widetilde{\overline{\tau}_x^*} = 0.04$ dPa). Otherwise as in Fig. 7.2.

stress, are generated farther east than in the control run and so take longer to reach the western boundary and reflect as Kelvin signals. The delayed negative feedback is therefore more attenuated by dissipation, and so takes longer to overcome the direct feedbacks in the eastern Pacific. This increased turnaround time is then reflected in an increased oscillation period.

Comparison of the transient responses

Given a transient disturbance, how quickly do the differences among these cases become apparent in the response? Fig. 7.5 shows simultaneous equatorial snapshots for the three cases during the first few months after perturbation. After only one month, the on- and off-equatorial thermocline looks nearly identical among the three cases—but significant differences are apparent in the entrainment temperature, with the warming of T_e strongest and farthest west in the strong-trades case, and weakest in the weak-trades case. By month 2, the strong-trades case shows the most rapid warming of SST, due to the stronger T_e anomalies at 140°W and the stronger effect of zonal advection acting on an enhanced $\overline{T}_x$. The weak-trades case, on the other hand, shows very little SST warming at month 2.

By month 3, it is possible to discern differences in the strengths of the equatorial zonal current and upwelling anomalies, which are strongest in the strong-trades case. One can also see differences in the equatorial wind stress response, with easterly anomalies forming over the east Pacific in the strong-trades case, while the other two cases show almost no stress anomalies in the east.

At month 4, there are clear differences in the thermocline structures for the west Pacific, where the strong-trades case shows a greater shoaling both on- and off-equator. By month 5, as this shoaling continues to affect the equatorial thermocline, the strong-trades case begins to show westward current anomalies developing in the east Pacific, while the other two cases continue to show little or no zonal current anomalies in the east. The zonal displacements of the stress responses are also clear at month 5, with the westerly stress anomalies (and associated upwelling, zonal currents, and zonal thermocline slope) farthest west in the strong-trades case and farthest east in the weak-trades case.

7.1.4 Change in the mixed layer heat budget

Which of the structural changes noted in the last section are *quantitatively* most relevant to the changes in ENSO? Fig. 7.6 shows the mixed layer heat budget along the equator for each of the three cases. This figure tracks changes at *fixed* locations, complementing the diagrams of Fig. 7.1 which followed the shifting position of peak SSTA variance. The middle row of Fig. 7.6, which corresponds to the control case, is essentially a rescaled version of Fig. 4.21 for reference. As the climate is altered, one can see substantial changes in the ENSO mechanism all along the equator.

110°W

In the far eastern Pacific, where the climatological thermocline is shallowest, the heat budget in the control run is quite simple. It consists essentially of two terms: $-\overline{w}\partial_z T'$ and

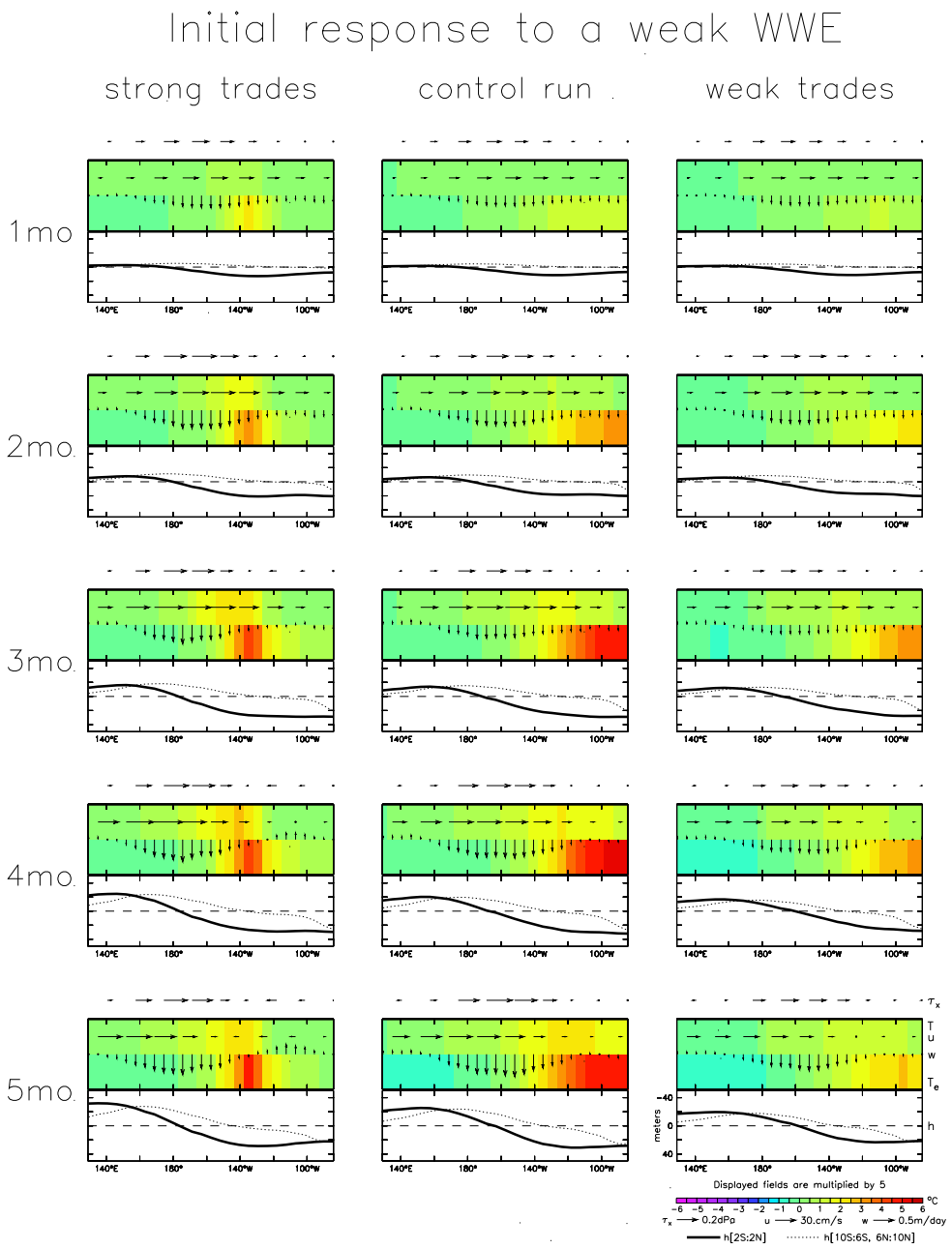

Figure 7.5: Comparison of the small-amplitude cases of Figs. 7.2–7.4, soon after the initial perturbation. Time flows down each column as a sequence of monthly snapshots, and all snapshots have the same scale (indicated in the bottom-right panel). Left column is the case with strengthened trades ($\widetilde{\overline{\tau}^*_x} = -0.1$ dPa), center column is the control case, right column is the case with weakened trades ($\widetilde{\overline{\tau}^*_x} = 0.04$ dPa).

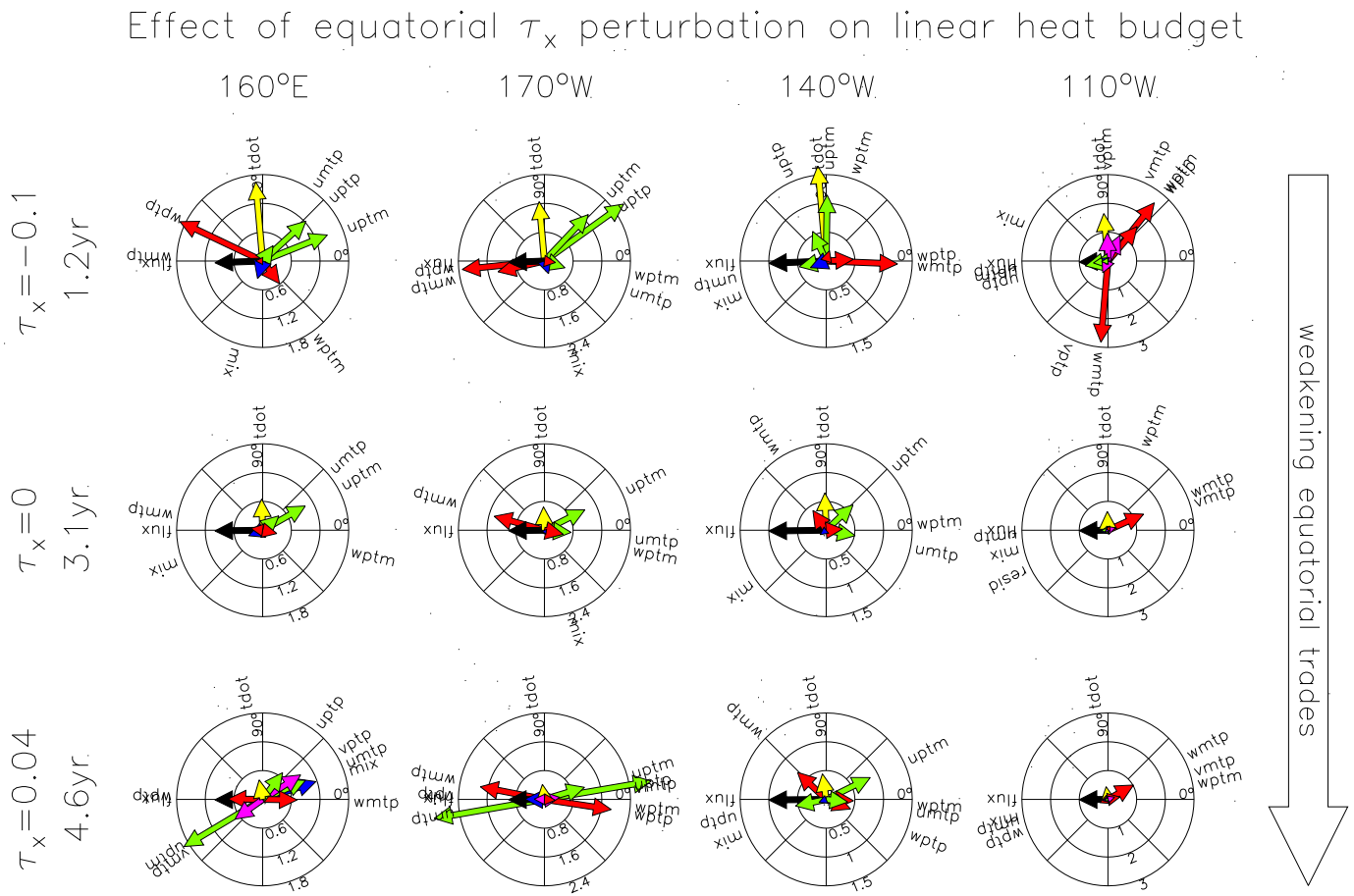

Figure 7.6: Comparison of equatorial mixed layer heat budget phasors for the small-amplitude cases of Figs. 7.2–7.4. The phasor diagrams are as described in Fig. 7.1 and Section 7.1.2. Middle row is the control case, top row is the case with strengthened trades ($\widetilde{\overline{\tau}^*_x} = -0.1$ dPa), bottom row is the case with weakened trades ($\widetilde{\overline{\tau}^*_x} = 0.04$ dPa). Each column corresponds to a given longitude, progressing from west on the left to east on the right. Diagrams at the same location, i.e. within a given column, have the same scale.

the surface heat flux. The $-\overline{w}\partial_z T'$ term leads local SSTA slightly, and is thus responsible for the oscillatory tendency in the east. There are only small contributions from $-\overline{u}\partial_x T'$ and $-\overline{v}\partial_y T'$, which stabilize and destabilize the oscillation, respectively.

For weakened climatological trades, the heat budget at 110°W remains quite simple, but there are important differences from the control case. The $-\overline{w}\partial_z T'$ term is relatively weaker than in the control run, due to the reduced $\partial_h T_e$ as a result of the deepened mean thermocline in the east. Because $-\overline{w}\partial_z T'$ is the dominant transitioning and growth mechanism, its reduced amplitude relative to surface flux results in a longer period and a greater damping rate for the oscillations. There is also a larger role for $-w'\partial_z \overline{T}$, since the equatorial zonal stress anomalies are displaced farther east than in the control run. This term is destabilizing, but has little effect on the oscillation period since it is nearly in phase with SSTA. Finally, the $-w'\partial_z T'$ term, which represents effects of reduced mean upwelling and $\partial_z T$, acts to further stabilize the oscillations and increase their period.

For strengthened climatological trades, the heat budget in the east is entirely different. Thermocline depth anomalies now *lag* local SSTA by a quarter cycle, and their effect on SSTA through $-\overline{w}\partial_z T'$ is much stronger relative to the surface flux than in the control run. The large anti-transitioning effect of this term, however, is more than compensated by changes in the meridional Ekman overturning circulation. Strong upwelling anomalies, induced by SSTAs farther west and acting on an enhanced $\partial_z \overline{T}$, overwhelm the effects of the thermocline depth variations to control the evolution of SSTA in the east. The transition between events is hastened by meridional advection, as warming south of the equator and weakening of the cross-equatorial currents occur a quarter-cycle ahead of the equatorial warming. Zonal advection plays a damping role at 110°W, which is as strong as the surface heat flux. The heat budget at this location is thus truly three-dimensional, and involves a very active set of competing processes which, amazingly, nearly balance and produce little net change in SSTA.

140°W

The heat budget at 140°W is generally more complex than at 110°W. In the control run, SST anomalies at 140°W are generated primarily by zonal advection, as eastward current anomalies appear prior to warm events and as SST changes farther east are advected westward by the climatological currents. The $-w'\partial_z \overline{T}$ term, an important destabilizer that is in phase with SSTA, becomes more active as one approaches the peak trade wind activity in the central Pacific. The $-\overline{w}\partial_z T'$ term plays more of a damping role at 140°W, as the SST changes induced by zonal advection have a larger effect on $\partial_z T$ than the subsurface changes induced by local movements of the deep thermocline. The thermocline motions do, however, induce a phase lag in the damping so that $-\overline{w}\partial_z T'$ remains important to the oscillation frequency.

In the weak-trades case, the zonal current variations at 140°W are stronger for a given SSTA than in the control case, due to the eastward shift of the wind response. These current anomalies, however, are much less effective at inducing SST anomalies, because of the weakening of $\partial_x \overline{T}$. The damping effect of $-\overline{w}\partial_z T'$ is also reduced by the weaker mean upwelling. The $-w'\partial_z \overline{T}$ term, on the other hand, plays a larger role due to the eastward shift of the wind variability.

In the strong-trades case, there is a very interesting budget at 140°W with clearly different roles for zonal and vertical advection. The anomalous zonal currents are in quadrature with local SSTA, so that $-u'\partial_x\overline{T}$ plays a purely transitioning role. The thermocline depth, on the other hand, is in phase with local SSTA and thus $-\overline{w}\partial_z T'$ plays a purely destabilizing role. One can think of $-u'\partial_x\overline{T}$ as the "inertia" for this oscillation and $-\overline{w}\partial_z T'$ as the power source: the oscillation passes through the zero-anomaly point due to the disequilibrium zonal currents, and then receives a boost due to advection on the anomalous thermocline at the event peak. The effects of these terms are further enhanced by the strong zonal SST gradient and strong equatorial upwelling in the strong-trades case, leading to a high-frequency, energetic oscillation at 140°W. The instability is largely balanced by the damping effect of incoming advection from farther east, where the SST anomalies are not as strong, and by the horizontal entrainment of off-equatorial waters by high-frequency eddies (here parameterized as horizontal diffusion).

170°W

At 170°W, near the peak of zonal stress variability, the control run shows even stronger roles for $-u'\partial_x\overline{T}$ and $-w'\partial_z\overline{T}$ which act to destabilize the oscillation. The damping effect of $-\overline{w}\partial_z T'$ is also stronger, because at this location (1) the thermocline depth hardly varies, and (2) $\partial_h T_e$ is weak because the climatological thermocline is deep. Thus the SSTA tends to dominate $\partial_z T'$, and the damping by $-\overline{w}\partial_z T'$ surpasses even the surface heat flux. The finite adjustment time of the active layer to the stress is again essential to the oscillation, as it induces a slight lead of the $-u'\partial_x\overline{T}$ term ahead of SSTA, and a lag of the $-\overline{w}\partial_z T'$ damping behind SSTA.

In the weak-trades case, the climatological thermocline flattens and the ENSO patterns shift eastward. In this case, the node in thermocline variability lies slightly *east* of 170°W, so the local thermocline is actually *elevated* when SST is warmer than normal. As this produces a strong $\partial_z T$ during warm events, one might expect mean upwelling to provide a strong damping for SSTA. This damping cannot materialize, however, because there is no mean upwelling at 170°W in the weak-trades case. A similar situation holds for zonal advection: although strong SST anomalies develop to the east, these cannot much affect 170°W due to the weakening of the mean zonal currents at that location. The zonal current anomalies do play an important destabilizing and transitioning role at 170°W but their effect is likewise attenuated by the reduction of the mean zonal temperature gradient. Anomalous upwelling plays a destabilizing role due to the proximity of the tradewind variability and the strengthening of $\partial_z\overline{T}$ at 170°W.

In the strong-trades case, the generation of SSTAs at 170°W is mostly due to zonal advection by anomalous currents, which act on an enhanced $\partial_x\overline{T}$. In contrast to the heat budget at 140°W, the $-u'\partial_x\overline{T}$ and $-u'\partial_x T'$ terms at 170°W lead local SSTA by substantially less than 90° phase, and therefore play destabilizing as well as transitioning roles. The SST anomalies generated by zonal advection are strongly damped by vertical advection, because in the strong-trades case (1) the mean upwelling is enhanced, (2) there is very little thermocline variability at 170°W, and (3) $\partial_h T_e$ is weak due to the deepened mean thermocline at 170°W.

160°E

In the far western Pacific, SST anomalies in the control run develop mostly due to zonal advection. The zonal current and SST gradient are weakest just prior to warm events, so that less and warmer water is advected in from the cold tongue. Anomalous upwelling also plays a small role as a destabilizer, due to the proximity of the tradewind variability. The SST changes induced by these processes are then damped by surface heat fluxes, horizontal mixing, and mean upwelling.

The weak-trades case is special, because SSTA in the west Pacific is out of phase with that in the eastern and central Pacific. Thus at 160°E, a local *warming* occurs during a La Niña event. Vertical advection cannot play any direct role at 160°E, because there is no net upwelling to convey T_e variations to the surface. The meridional currents are also weak in this case, and so cannot much affect the equatorial temperature despite the reasonably strong meridional temperature gradients that develop. The net effect of zonal advection is also weakened due to the lack of strong temperature gradients. As a result, there is very little SSTA variability at 160°E. The SSTAs that *do* develop are mostly transported in by the mean zonal currents and horizontal mixing from farther east, where weak upwelling generates warm anomalies during La Niña, as the thermocline deepens in the west.

The strong-trades case at 160°E is dynamically more interesting. Here the warm anomalies are generated by zonal advection on the strong $\partial_x T$, amplified by strong zonal current anomalies associated with the resonant coupled Rossby wave. In contrast to the control run, there is now mean easterly stress and upwelling at 160°E. The water is entrained into the mixed layer from below remains relatively unperturbed due to the deep climatological thermocline, and thus has mainly a damping effect on local SSTA. Following the peak warming there is a slight reduction in upwelling which opposes the transition to the cold event, but this is more than compensated by the slight phase lag of the T_e cooling behind the local surface warming, which hastens the transition.

Discussion

There are several key points to take from Fig. 7.6. The mixed layer heat budget in the intermediate model is complex, with significant contributions from surface fluxes, vertical advection, and zonal advection, and even meridional advection and mixing at various points along the equator. This complexity may provide a clue as to how ENSO can behave so differently in different models. As the total SSTA tendency is a small residual of many large tendency terms, a relatively small change in any given term can have a significant impact on the oscillation amplitude and period. In particular, the surface heat flux, which tends to be heavily parameterized in the current generation of climate models, appears to be a first-order term in the ENSO heat budget nearly everywhere along the equator.

What maintains the ENSO amplitude? The power source for the oscillation, ultimately, is the sun, which heats the ocean surface. The warm ocean then warms and moistens the overlying atmospheric boundary layer. Differential heating of the atmospheric boundary layer produces horizontal pressure gradients at the surface, which contributes to the generation of surface winds. The moist air also represents a vast reservoir of latent heat, which is

gathered up by the circulation, focused into convective regions, and tapped upon condensation of water vapor into cloud droplets. The differential heating of atmospheric columns above the boundary layer contributes to the horizontal pressure gradients at the surface, driving additional winds which then affect the oceanic thermocline, currents, and surface temperature. The statistical atmosphere parameterizes the variations in the strengths and locations of boundary layer heating and convective heating into a simple relationship between the SST and wind stress anomalies, whereby warm anomalies in the east generate westerly stress anomalies over the central Pacific. The ENSO *amplitude* is then maintained by a positive feedback cycle, whereby deepening of the thermocline in the east acts through climatological Ekman overturning to warm the surface, which induces westerly stress anomalies that further deepen the thermocline in the east. One can think of ENSO as self-regulating the conversion of thermal and latent energy (provided by the sun) into the mechanical work and available potential energy fluctuations associated with the oscillation.

What sets the ENSO period? Ocean-atmosphere feedbacks provide not only an essential power boost, but also off-equatorial wind stress curl that pumps water between the equator and off-equator to facilitate the transitions between events. The continents are also important, as they reflect wave signals back and forth across the basin; when local feedbacks dominate, as in the case with strong trades, basin resonance of coupled Rossby waves can be essential to the ENSO period. Advection by the anomalous equatorial zonal currents ($-u'\partial_x\overline{T}$), which is associated with the meridional curvature of the equatorial thermocline and the propagation of equatorial waves, appears to be a key mechanism in the transitions between warm and cold events, and is largely what sets the oscillation period. The related slow adjustment of the zonal-mean thermocline depth, which is associated with the equatorial recharge/discharge of heat content, is also important in the transition, as it tends to produce a phase lead of vertical advection ($-\overline{w}\partial_z T'$) ahead of SST anomalies in the east Pacific.

The heat budget in the weak-trades case closely mirrors that of the control run in the eastern Pacific, although important differences are apparent in the western/central Pacific. The weakening of the zonal SST gradient in this case reduces the transitioning role of zonal advection, which leads to a decrease in the oscillation frequency. Deepening of the thermocline in the east Pacific, furthermore, reduces the destabilizing role of vertical advection, which leads to stronger damping of the oscillation and also shifts the position of maximum variability eastward where the entrainment temperature is most sensitive to thermocline depth.

In the strong-trades case, on the other hand, the strengthening of the zonal SST gradient enhances the transitioning role of zonal advection. This leads to an increase in the oscillation frequency, and the saturation of the entrainment temperature in the eastern Pacific shifts the peak variability into the central Pacific. The short period of this mode is nearly resonant with coupled Rossby waves, and so one can see westward propagation of SST anomalies in the eastern and western Pacific.

One interesting observation from Fig. 7.6 is that climate changes affect not only the *magnitude* of the tendency terms, but also their *phase* relative to local SSTA, which alters their roles in the oscillation. The role of $-u'\partial_x\overline{T}$ at 140°W, for example, goes from destabilizing to transitioning as the trades strengthen. This then affects the sensitivity to

further climate changes. For weak trades, changes in $\partial_x \overline{T}$ alone will have little effect on the oscillation frequency, since in this case it is the thermocline variations (not the zonal currents) that bring about the transition. For strong trades, on the other hand, the zonal current variations are the key transition mechanism and changes in $\partial_x \overline{T}$ can have a major effect on the oscillation frequency.

The heat budget phasors can also yield useful information on *what* and *where* to observe the real ocean and atmosphere in order to improve modeling and forecasting of ENSO. If the SSTA evolution at a given location is most strongly dependent on $-u'\partial_x \overline{T}$ for the transition, then by monitoring the anomalous zonal currents at that location (either directly or through a proxy like sea level) one can effectively anticipate changes in SST. And if SSTA *growth* is found to depend strongly on $-\overline{w}\partial_z T'$, one may be able to identify weak-upwelling conditions with conditions of high predictability. The climate sensitivity experiments also indicate that the ENSO observing system and modeling requirements may change if the climate changes.

Finally, the phasor diagrams are an excellent diagnostic for comparing numerical models to each other and to observational analyses, and for identifying parts of a simulation that require improvement for more realistic ENSO variability. Although different models may have similar-looking ENSOs when one looks only at equatorial SST, they may have very different mechanisms and therefore different sensitivities to climate change. Phasor diagrams of the mixed layer heat budget are one way to verify that a model is simulating the "right" kind of ENSO for the right reasons.

7.1.5 Responses to other climate perturbations

Having examined the prototype tradewind-strength case in detail, we next ask: To what extent does this prototype mirror the effects of other climate perturbations? Fig. 7.7 summarizes the effects on ENSO of all the perturbations discussed in Chapter 5. Panel (a) corresponds to the imposed zonally-uniform change in the strength of the equatorial trades that we have examined so far: as the trades weaken, the oscillation period increases and the variability shifts eastward, consistent with the analysis of Section 7.1. The amplitude is greatest when the trades are very strong or near-normal, and weakest when the trades are weak or only moderately strengthened.

Radiative forcing

Panel (b) shows the ENSO response to an imposed basinwide change in the surface heat flux. Chapter 5 showed that since the climate response to uniform heating produces a strengthening of the zonal SST gradient and associated zonal stress, the resultant climate change is very similar to that for an imposed change in the strength of the equatorial trades. Panel (b) indicates that the ENSO change is similar as well. With increasing heating, the climatological trades weaken, the ENSO period lengthens and the SST variability shifts eastward. There are two active regimes associated with the zonal-advective mode (for strong heating) and the vertical-advective mode (for weak heating), and two inactive regimes (for cooling or for moderate heating). The ENSO-mapping between (a) and (b) is similar to the climate-mapping between Figs. 5.6 and 5.13, with a 10 Watt m^{-2} heating

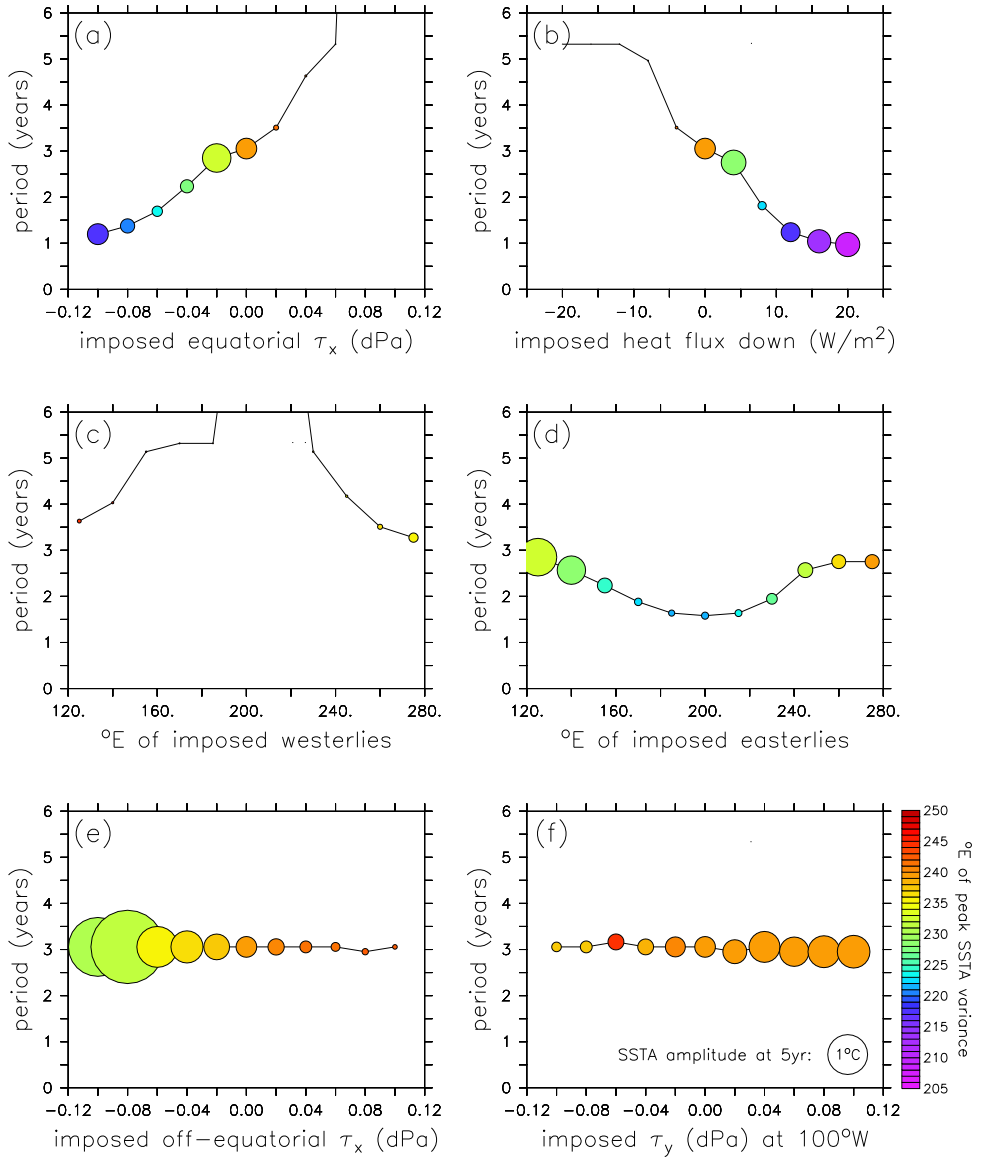

Figure 7.7: Changes in the intermediate model ENSO for the climate perturbations of Chapter 5. Abscissa gives the (a) imposed zonally-uniform zonal stress at the equator, (b) imposed heat flux into the ocean, (c) longitude of local weakening of the equatorial trades, (d) longitude of local strengthening of the equatorial trades, (e) imposed zonally-uniform zonal stress off-equator, and (f) imposed meridional stress in the eastern Pacific. Ordinate gives the ENSO period, dot color the longitude of peak equatorial SSTA variance, and dot radius the SSTA oscillation amplitude at this longitude, 5 years after the imposition of a weak westerly stress anomaly in the central Pacific. The key to dot size and color for all panels is given in (f).

giving roughly the same change as an imposed 0.06 dPa easterly stress.

Longitude of the stress

Panels (c) and (d) show the importance of the zonal position of an equatorial τ_x perturbation. Chapter 5 showed that the effect of a stress perturbation on the coupled climatology is greatest when it lies over the central basin, where it can effectively seed coupled feedbacks by altering both the extent of shallow thermocline in the east and the strength of equatorial upwelling in the east Pacific region of shallow thermocline. Here we see that the effect on ENSO is likewise greatest when the τ_x perturbation lies in the central basin. Off-center perturbations affect the ENSO amplitude and longitude slightly more when they are in the west than in the east, since the east Pacific thermocline depth and central Pacific zonal SST gradient are more responsive to perturbations in the west (Figs. 5.11 and 5.12).

Off-equatorial stress

Panel (e) shows the effect of an off-equatorial zonal stress perturbation on the simulated ENSO. As the off-equatorial trades weaken, the variability weakens and shifts eastward. Interestingly, the ENSO *period* is hardly affected by such a perturbation. When the off-equatorial trades are strong enough, the climatology becomes unstable and a limit cycle develops.

Meridional stress

Panel (f) shows the effect of a change in the cross-equatorial southerlies in the eastern Pacific. The period is hardly affected, and there are only small changes in the amplitude and position of the variability, with ENSO strengthening only slightly as the southerlies strengthen.

Similarity of the results

Recalling that Chapter 5 showed that coupled feedbacks tend to homogenize the climate response, it is interesting to compare results from the various ENSO sensitivity experiments on a common footing. Fig. 7.8 overlays the results from all the experiments in Fig. 7.7 as a function of the strength of the climatological trades in the central Pacific. The results lie essentially along the same curve, indicating that the period is a fairly robust function of the coupled trade wind strength regardless of the type of imposed perturbation. The strongest amplitudes occur at near-normal and very strong trades, and the weakest amplitudes at weak and moderately strong trades, just as in the prototype case that we have examined in detail. And for the most part, the ENSO variability at strong trades and short periods occurs farther west than that at weak trades and long periods.

The off-equatorial τ_x-perturbation case is something of an exception, in that the period changes less rapidly with the equatorial trades while the amplitude changes more rapidly. Recall that the off-equatorial stress can only *directly* affect the *zonal-mean* depth of the equatorial thermocline. A zonally-uniform change in thermocline depth induces less of a change in zonal SST gradient than does a change the slope of the thermocline, and therefore

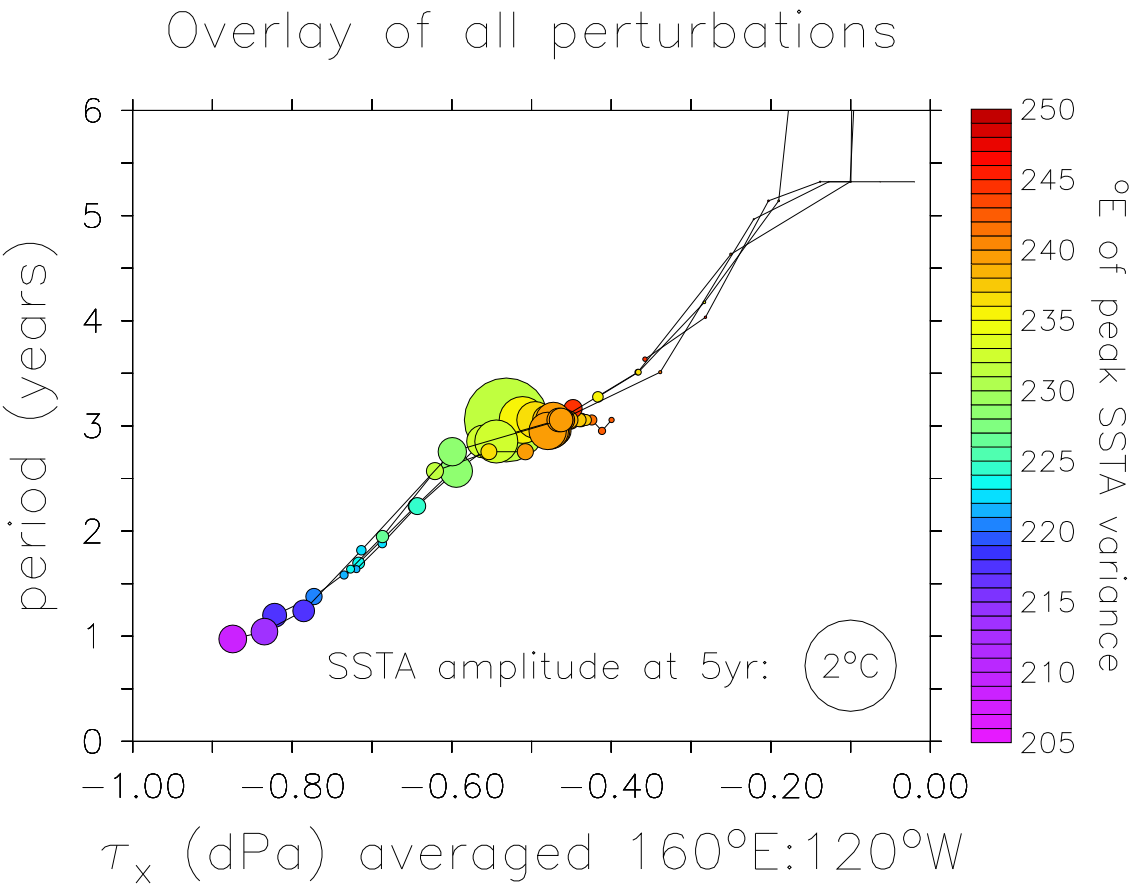

Figure 7.8: Linear ENSO properties as a function of the strength of the equatorial trade winds, for all of the climate-change cases examined in Chapter 5. Horizontal axis is the mean zonal stress (averaged over the region 170°E–120°W, 2°S–2°N), vertical axis is the oscillation period. Dot radius is proportional to the amplitude of the oscillation 5 years after the imposition of a transient westerly stress perturbation. Dot color indicates the longitude of peak equatorial SST anomaly variance.

results in a smaller change in zonal stress with weaker coupled feedbacks. The upshot is that compared to an imposed change in the equatorial trades, an imposed change in the off-equatorial trades induces a larger change in the subsurface temperature structure relative to the surface temperature structure. Now recall that $-u'\partial_x\overline{T}$ is a transitioning mechanism which depends exclusively on the mixed layer SST gradients, while $-\overline{w}\partial_z T'$ is more of a destabilizing mechanism which depends on the subsurface structure. Examination of the heat budget phasors for the off-equatorial case (not shown) confirms that there is a larger change in $-\overline{w}\partial_z T'$ relative to $-u'\partial_x\overline{T}$, and consequently a greater effect on the amplitude than the period, than in the equatorial case.

Despite this, Fig. 7.8 is remarkable because it shows that in the coupled context, ENSO behavior is determined primarily by strength of the equatorial trades—the "El Niño-ness" or "La Niña-ness" of the climatology. This confirms the relevance of the prototype case, and allows us to forgo detailed analysis of the other climate-change cases. Instead, we turn to the effects of climate change on ENSO in nonlinear and stochastic regimes.

7.2 Nonlinear regime

The previous section focused on ENSO behavior in the small-amplitude regime, and at a value of air-sea coupling where unforced oscillations are damped. In this section, we consider the effect of increasing coupling, which tends to destabilize the oscillations and allows them to grow large enough that nonlinearities become important. We also take a step closer to the stochastic context, by examining the response of the system to strong transient wind stress disturbances.

7.2.1 ENSO sensitivity at increased coupling

Is the ENSO sensitivity to climate any different if the wind stress depends more strongly on SST anomalies? This is an important question, since (1) the strength of the stress response in the real world is unclear, due to sparse observations and uncertain analyses; (2) the effective "coupling strength" may vary with time, due to changes in the mean state and ENSO structure; and (3) current atmospheric models have a range of different stress responses to SSTAs.

Fig. 7.9 shows how the strength μ of the wind stress anomaly response to SSTAs affects the intermediate model sensitivity to the trade winds. At the standard coupling ($\mu = 1$) ENSO is damped, except at very strong climatological trades where a weak 1.2-year oscillation is sustained. As coupling increases, another sustained regime appears, with a period of about 3 years at near-normal trades. Around $\mu = 1.07$, these two regimes merge and there are sustained oscillations for all $\widetilde{\tau}_x^* < 0.02$ dPa, with period increasing as the trades weaken. As coupling increases further, so do the amplitude, period, and skewness of the oscillations, as well as the critical tradewind strength required for sustained variability.

Thus it appears that the lengthening of the period with a weakening of the trades is robust to large changes in coupling, even as the oscillations grow large enough to feel the influence of nonlinearity. The stability structure is also fairly robust to moderate changes in coupling, with peak ENSO growth/amplitude at strong and intermediate trades. Note that

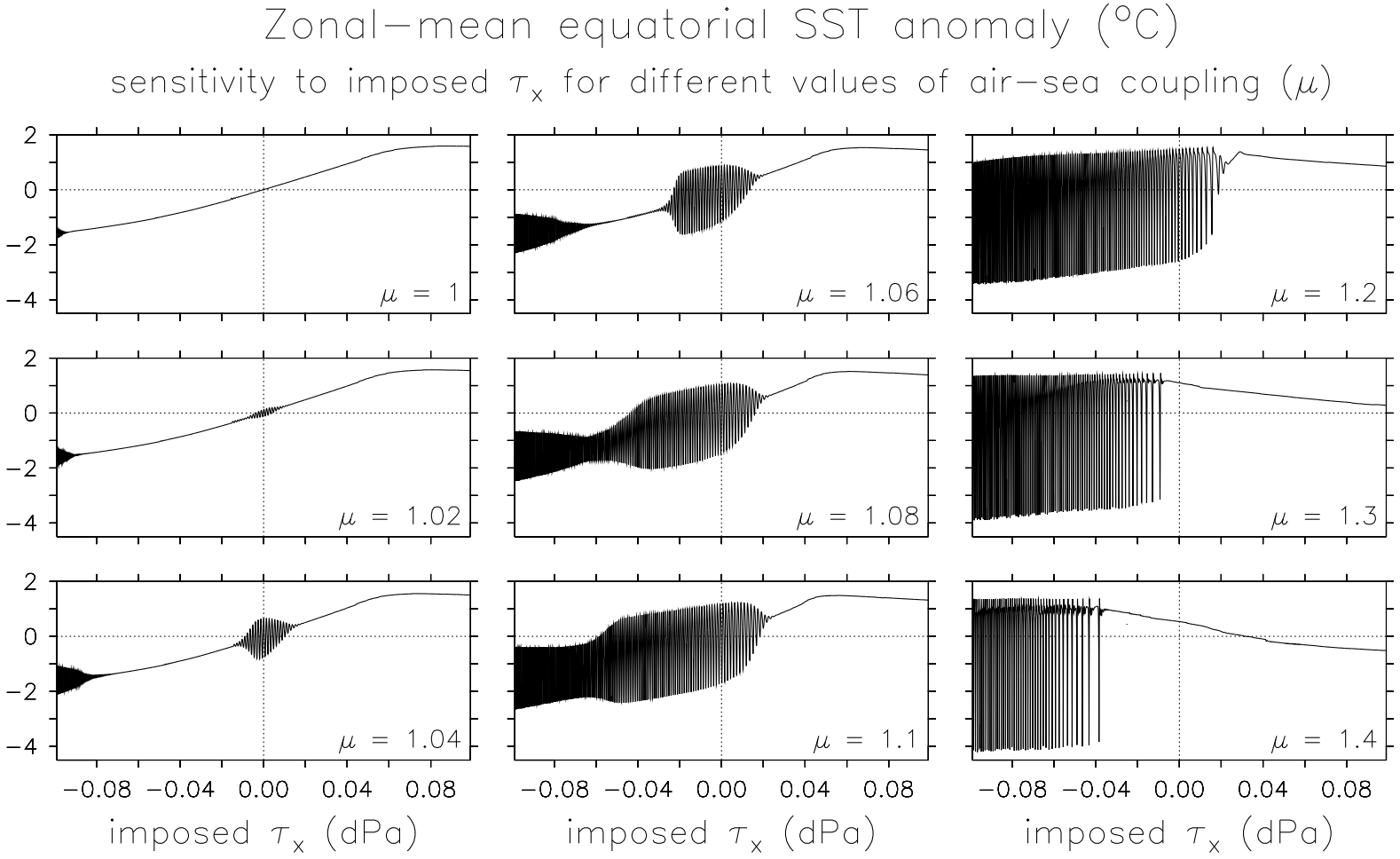

Figure 7.9: ENSO sensitivity to the time-mean strength of the trade winds, for different air-sea coupling strengths. Each panel shows zonal-mean equatorial (2°S–2°N) SST anomalies from a 500-year run of the intermediate model, in which the mean equatorial trade winds are gradually weakened over the course of the simulation. The imposed zonal stress perturbation is given on the horizontal axis, with tic marks every 0.02 dPa (50 years).

even with a coupling strength 40% higher than the standard value, sustained oscillations cannot exist when the trades are very weak.

As an aside, note that at very strong coupling the zonal-mean climatological SST actually *cools* as the imposed τ_x perturbation becomes more westerly. In this case, feedback easterlies in the western Pacific induce upwelling on the shallow thermocline there, which cools the surface. This induces more easterlies slightly west of the cooling, and creating a positive feedback cycle that generates a cold tongue in the central Pacific instead of the eastern Pacific.

7.2.2 Response to strong transient wind events

Does the ENSO response to *strong* transient wind stress differ from its response to weak stress disturbances? And how does this response change as climate changes? This section addresses these questions in the context of the intermediate model.

Fig. 7.10 shows how the intermediate model response to strong wind stress kicks changes as the climatology changes. A westerly kick (top panel) generally produces an initial warming, an easterly kick (bottom panel) a cooling. Following the first cycle, the oscillations decay away much as in the small-amplitude case (Fig. 7.1), and also reflect the stability properties at moderately higher coupling (Fig. 7.9). As the mean trades weaken, the oscillation period increases and the damping rate exhibits local minima for strong and near-normal mean trades. For very weak trades, there is essentially no lasting response to transient stress.

Fig. 7.11 focuses more closely on the initial SSTA cycle following a stress kick. For weak kicks (column a), the system is approximately linear and easterly and westerly kicks induce nearly opposite responses. The initial zonal-mean SSTA response corresponds to about 10°C per dPa of stress kick for strong mean trades, 13°C/dPa at normal trades, and less than 2°C/dPa at weak trades. Since the transient behavior is a superposition of normal modes, some of which decay rapidly but project strongly on the initial disturbance, the timing of the first peak is not directly tied to the period of the least-damped mode. Indeed, the bottom panel of (a) shows that the timing of the first peak is nearly independent of the tradewind strength, while the period of the least damped mode (roughly the time between the first and third extrema) varies strongly with the tradewind strength.

Is the response to strong kicks any different? Comparing (b) to (a) in Fig. 7.11, it is clear that a 0.2 dPa kick is generally less efficient at generating SSTA disturbances than is a 0.02 dPa kick. Some exceptions are at strong trades, where strong westerly kicks are more efficient than weak westerly kicks at inducing initial warming (W1), and at weak trades, where strong easterly kicks are more efficient than weak easterly kicks at inducing initial cooling (E1). The amplitude of the third peak relative to the kick (W3, E3), indicates that for strong-to-moderate climatological trades, strong kicks are roughly half as efficient as weak kicks at putting energy into the least-damped mode.

How is the *timing* of the response affected by nonlinearity? The answer is illustrated by the bottom row of Fig. 7.11. For near-normal tradewind strengths, the first El Niño following an easterly kick (E2) occurs several months sooner than in the linear case. For strong trades, the initial El Niño following a westerly kick (W1) is delayed about a month relative to the linear case, while the initial La Niña following an easterly kick (E1) comes

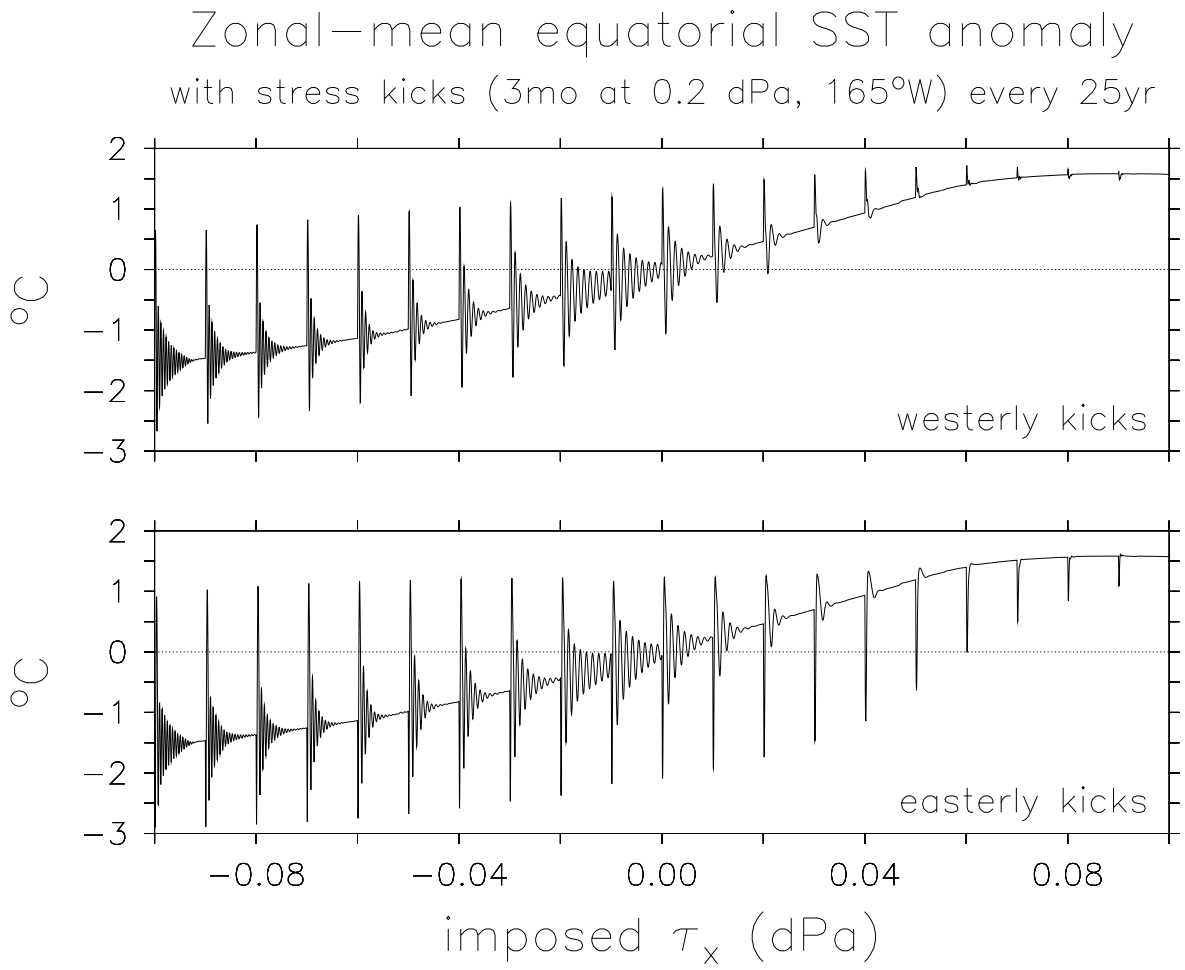

Figure 7.10: Simulated ENSO response to transient wind events. Zonal-mean equatorial (2°S–2°N) SST anomalies are shown from a 500-year run of the intermediate model, during which the mean equatorial trade winds are gradually weakened (horizontal axis indicates the imposed zonal stress perturbation). Meanwhile, the system is subjected to a series of transient wind stress events which occur every 25 years. Top panel shows the response to westerly events, bottom panel shows the response to easterly events. Each stress event lasts for 3 months and has a bivariate Gaussian spatial structure, with a peak amplitude of 0.2 dPa on the equator at 165°W, and e-folding halfwidths of 40° longitude and 10° latitude.

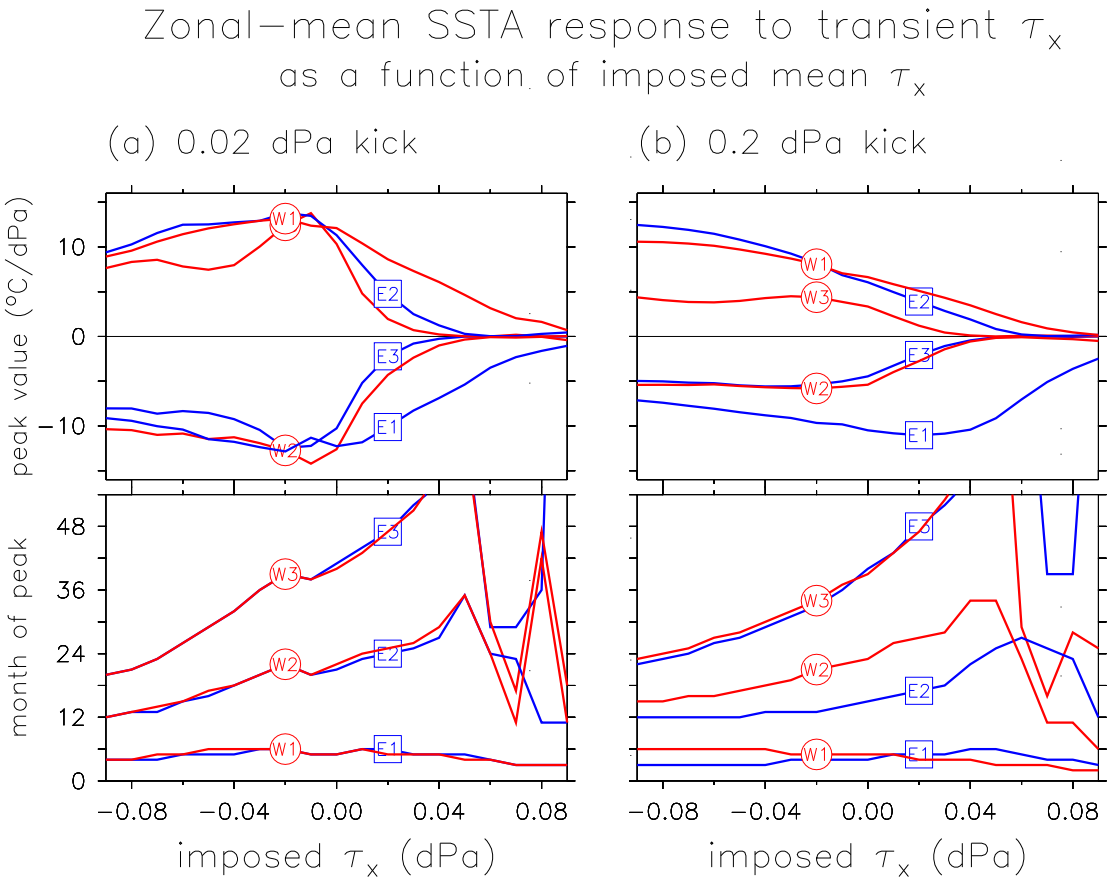

Figure 7.11: Transient response statistics for zonal-mean equatorial SST anomalies, as a function of the climatological tradewind strength. As in Fig. 7.10, the intermediate model is subjected to a series of transient stress kicks, whose peak values are given at the top of each column: (a) is for the weak kicks of Section 7.1 and (b) is for the stronger kicks of Fig. 7.10. Horizontal axis gives the imposed *climatological* stress perturbation at the time of the kick. Top row gives the first three SSTA extrema following the stress kick, and bottom row gives the months they occur. For a westerly kick, W1 indicates the first event (warm), W2 the second (cold), and W3 the third (warm). For an easterly kick, E1 indicates the first event (cold), E2 the second (warm), and E3 the third (cold).

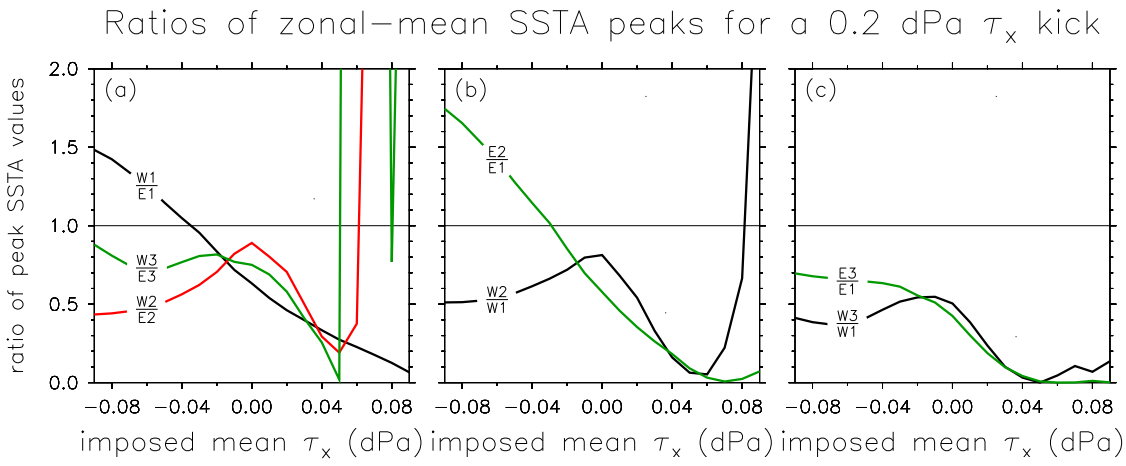

Figure 7.12: Ratios of magnitudes of the peak zonal-mean SST anomalies shown in the upper-right panel of Fig. 7.11. Horizontal axis gives the imposed climatological stress perturbation.

roughly a month sooner than in the linear case. For weak trades, the responses shift in the opposite sense, with E1 occurring slightly later than W1. Thus although the linear period grows *longer* as the trades weaken, the first warm event actually appears progressively *sooner* following a strong westerly kick. Despite these changes in the transient behavior, the phase of the modal response (W3, E3) is remarkably insensitive to the strength of the kick, or to whether it is easterly or westerly.

How does the initial SSTA response to a strong westerly kick differ from that for an easterly kick? In addition to the timing differences noted above, there are also substantial differences in amplitude. Panel (a) of Fig. 7.12 shows ratios of the SSTA peak responses for westerly versus easterly kicks. Focusing on the first SSTA peak (W1, E1), we see that for strong trades, a westerly kick induces a stronger initial peak than does an easterly kick. As the trades weaken, westerly kicks induce progressively weaker initial peaks relative to easterly kicks, and at very weak trades the westerly kicks have almost no effect. Note that this change is related to the skewness change evident at higher coupling (Fig. 7.9). The same nonlinearities are responsible in both contexts: if the trades are too strong, easterly kicks cannot affect SST due to the outcropping of the thermocline in the east; if the trades are too weak, westerly kicks cannot affect SST due to the absence of mean upwelling at the equator.

Focusing on the second and third SSTA peaks, it is clear that at the strong-to-intermediate tradewinds where such peaks occur, they tend to be stronger for easterly kicks than for westerly kicks. In the stochastic context, at strong trades one can expect more "modal" variability to arise from easterly kicks, but more "transient" variability to arise from westerly kicks. This is also evident in panel (c), which compares the third SSTA peak to the first.

How strong is the immediate aftermath of the initial event? The answer again depends on the strength of the climatological trades. It is evident from Fig. 7.9 that for strong

trades, the first warm event after a westerly kick is more than twice as strong as the subsequent cold event. As the trades weaken, the cold aftermath disappears, until for very weak trades there is almost no initial warming and instead only a slight cooling in response to a westerly kick. Panel (b) of Fig. 7.12 summarizes such changes by showing the ratios W2/W1 and E2/E1. For strong trades, an easterly kick induces a much stronger aftermath than does a westerly kick. In this case the warm aftermath of the easterly kick is stronger than the initial cold event; in fact, as can be seen in panel (b) of Fig. 7.11, it is stronger even than the initial warm event following a westerly kick! As the mean trades weaken, the warm aftermath of an easterly kick becomes progressively weaker relative to the initial cold event. The cold aftermath of a westerly kick, however, shows a local maximum relative to the initial warming when the trades are near-normal. For very weak trades, an easterly kick produces a fairly strong initial cold spike without any warm aftermath, while a westerly kick produces hardly any response.

Having considered the effect of individual stress disturbances on the ENSO system, we are now prepared to enter a more realistic regime—one that includes continual excitation by random wind stress variability.

7.3 Stochastic regime

In this section, we consider the effects of climate changes on a stochastically-excited ENSO. This context is arguably more realistic than those we have considered so far, given the large intraseasonal wind stress signals present in observational analyses (Chapter 2). The two key questions are: (1) Do the changes in the modal and transient behavior we have seen up to this point also apply in stochastic regime? and (2) How large a climate change must occur before its effect on ENSO can be distinguished from natural variations?

To answer these questions, we take advantage of the stochastic hybrid coupled intermediate model developed in Chapters 3 and 4. Noise of moderate amplitude is used (as in Fig. 4.32 and Chapter 5), so that the ENSO variability mimics the amplitude, distribution, spectrum, and spectral variations of observed SST anomalies (Fig. 2.11). The climate-change cases correspond to the 500-year stochastic runs of Chapter 5, in which the strength of the equatorial trades are gradually weakened over the course of the simulation. To ensure good statistics for the hypothesis tests, a 5000-year control run is also performed in which no climate perturbation is imposed.

7.3.1 Overview of the stochastic timeseries

Control run

The first 500 years of the 5000-year stochastic control run are shown in Fig. 7.13. There are rather strong natural fluctuations in the strength of the ENSO activity from decade to decade, and from century to century. That these fluctuations are due entirely to the statistically-steady noise forcing illustrates a key point: in the stochastic context, temporal variations in ENSO behavior may arise from pure chance, and need not be due to fundamental changes in the climate system. Thus any suspected effect on ENSO of an

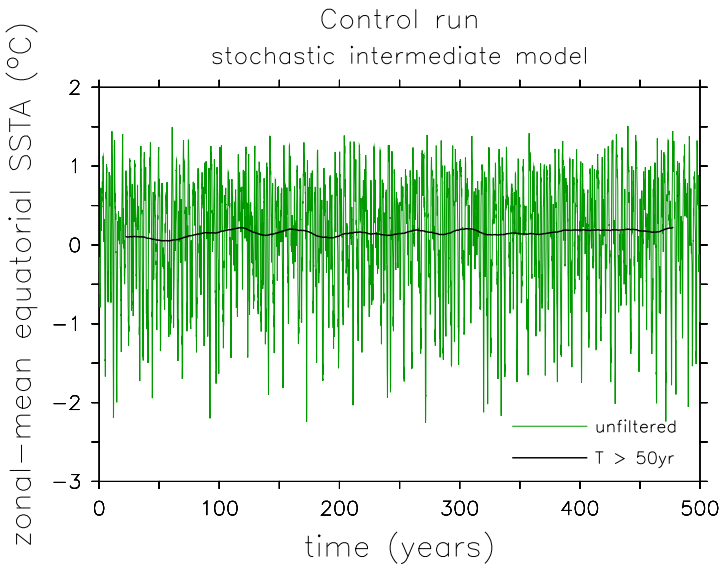

Figure 7.13: Zonal-mean equatorial (2°S–2°N) SST anomalies from a 500-year control run of the stochastic intermediate model. Green line is the monthly anomaly timeseries; black line filters out periods shorter than 50 years.

imposed climate forcing should always be tested against a hypothesis of no climate change at all.

Effect of changing equatorial trades

Fig. 7.14 shows how the stochastic model responds to a change in the strength of the trade winds. The horizontal axis is the same as in Fig. 7.13, but has been relabeled to indicate the strength of the imposed climatological zonal stress perturbation. Note that the simulations of Figs. 7.13 and 7.14 are driven by the same particular realization of the wind stress noise, so any differences between the two timeseries must arise entirely due to the imposed mean zonal stress and associated dynamical changes.

As the trade winds weaken, the equatorial band warms up; it is apparent that the climate response is nonlinear, i.e. that the long-term mean SST is less sensitive to strong $\overline{\tau}_x$ perturbations than to weak ones. Also as the trades weaken, ENSO becomes less active. The ENSO behavior at weak trades appears to be quite different from anything in the control run, so the climate perturbation does indeed appear to have an impact on ENSO. The remaining sections will refine and quantify these statements.

7.3.2 Distribution

The quantiles of zonal-mean equatorial SST anomalies from the control run are shown in Fig. 7.15. The shaded bands indicate the uncertainty that results from trying to characterize the quantiles using timeseries of various lengths. The sample quantiles for a 10-year timeseries are highly variable, suggesting that it may be difficult to see the effects of climate

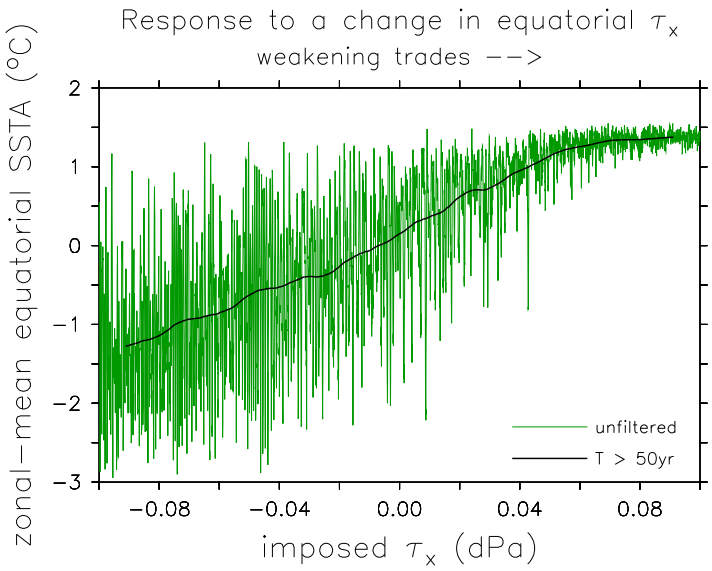

Figure 7.14: Simulated response of equatorial Pacific SST to a change in the strength of the trade winds. The imposed zonal stress perturbation is zonally constant and has a meridionally Gaussian shape with an e-folding halfwidth of 15°. Horizontal axis indicates the amplitude of the imposed zonal stress, which changes linearly from −0.1 dPa (easterly) to 0.1 dPa (westerly) over the course of a 500 year stochastic simulation. Otherwise as in Fig. 7.13.

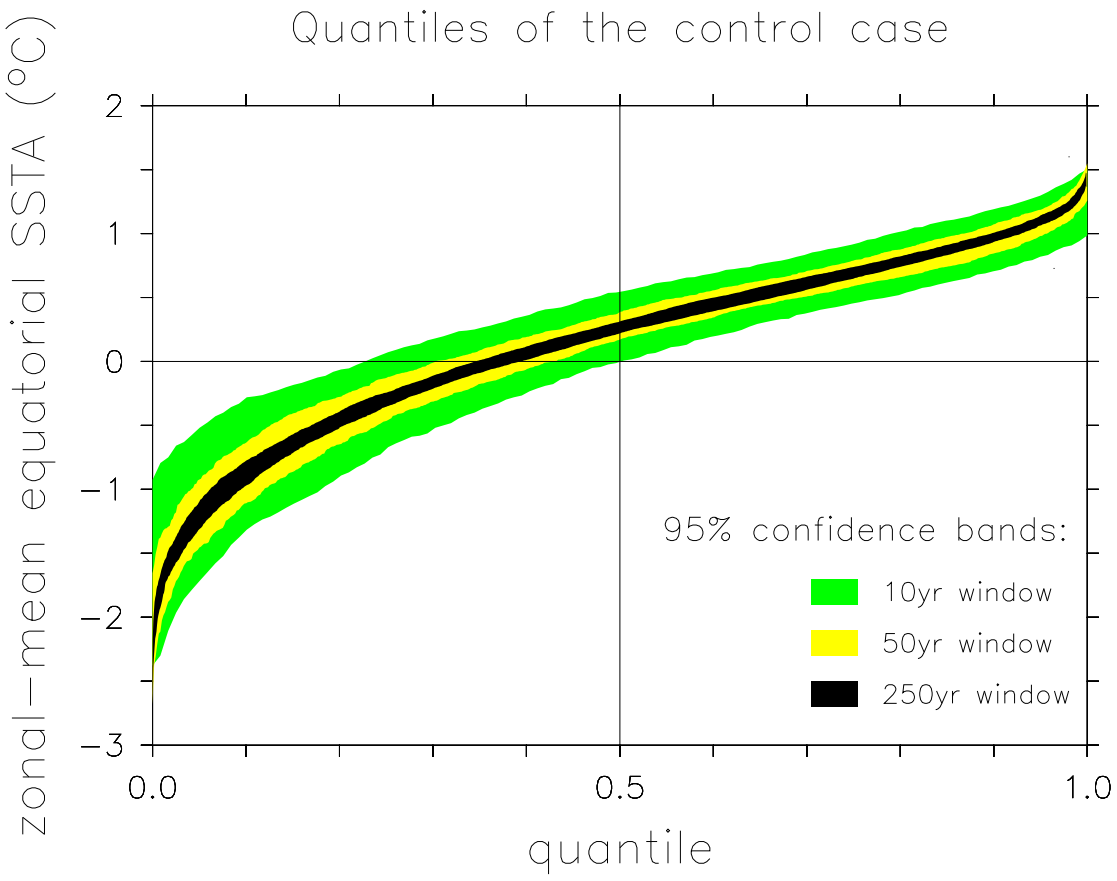

Figure 7.15: Quantile function for zonal-mean equatorial (2°S–2°N) SST anomalies, based on the control run of the stochastic intermediate model. Horizontal axis indicates the fraction of SSTA values smaller than the value given on the vertical axis. The shaded bands are 95% confidence intervals for the quantiles, based on a 5000 year simulation divided into non-overlapping windows of length 10 years (green), 50 years (yellow), and 250 years (black). Thus the green band indicates that for any given 10 year timeseries, to 95% confidence the coldest SSTA will lie between −2.7°C and −0.7°C, the median between −0.1°C and 0.6°C, and the warmest between 0.9°C and 1.5°C.

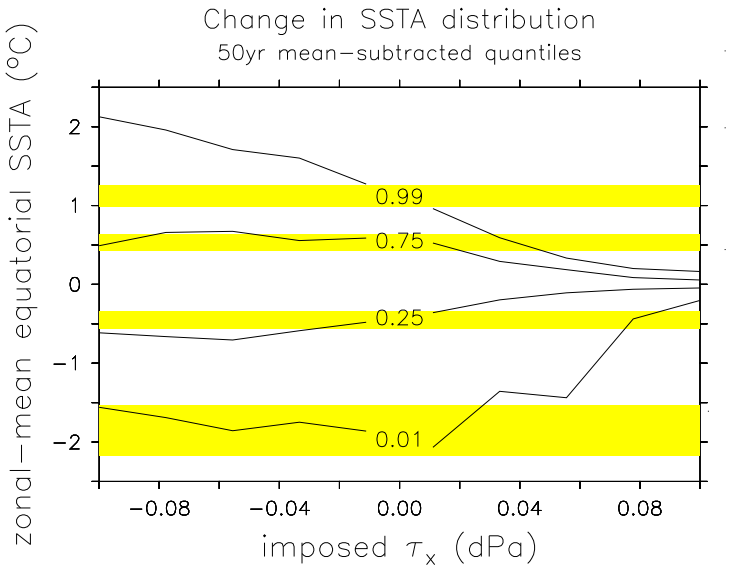

Figure 7.16: Change in the distribution of zonal-mean equatorial (2°S–2°N) SST anomalies, for the experiment of Fig. 7.14. The 500-year simulation is divided into 10 non-overlapping windows, each of length 50 years. For each window, the mean is subtracted and then the quantiles are computed and plotted (solid lines). Repeating this procedure in the 5000-year control run yields 95% confidence bands (shaded) for the unperturbed 50-year quantiles.

change on the distribution at these time scales. To reliably detect changes in the SSTA distribution, it clearly helps to have long timeseries.

The cold-skewness of the control-run SSTAs is evidenced by the shift of the median above zero, and by the stronger amplitude of cold events relative to warm events. (Note that *observed* SSTAs over the last century appear to be skewed toward *warm* events, rather than cold events as in the model; thus the quantile function for the observations would resemble an upside-down version of Fig. 7.15.) The confidence intervals are widest at the lowest quantiles, indicating that a shift in the cold events (here the strong La Niñas) will be harder to detect than an equivalent shift in the median or warm events.

How does the distribution of these SST anomalies change as climate changes? Fig. 7.16 shows what happens to the SSTA quantiles as the trades weaken. A 50-year running mean has been subtracted from the quantiles so that changes are easier to see, and the shaded bands indicate the control-run confidence bands for 50-year timeseries. For strong trades, warm events are significantly strengthened compared to the control, and the SSTA distribution becomes positively skewed; changes in the magnitude of the coldest 1% of events, however, are not detectable even at 50-year timescales. For weak trades, ENSO is significantly weakened and the SSTA distribution becomes even more negatively skewed than in the control. In the weak-trades case, all four quantiles are significantly different from those in the control run, and the changes in the most extreme events can be detected even with 10-year timeseries. In short, the change in distribution due to ENSO *suppression* (for weak trades) is more easily detected than that due to ENSO *conversion* from a slow

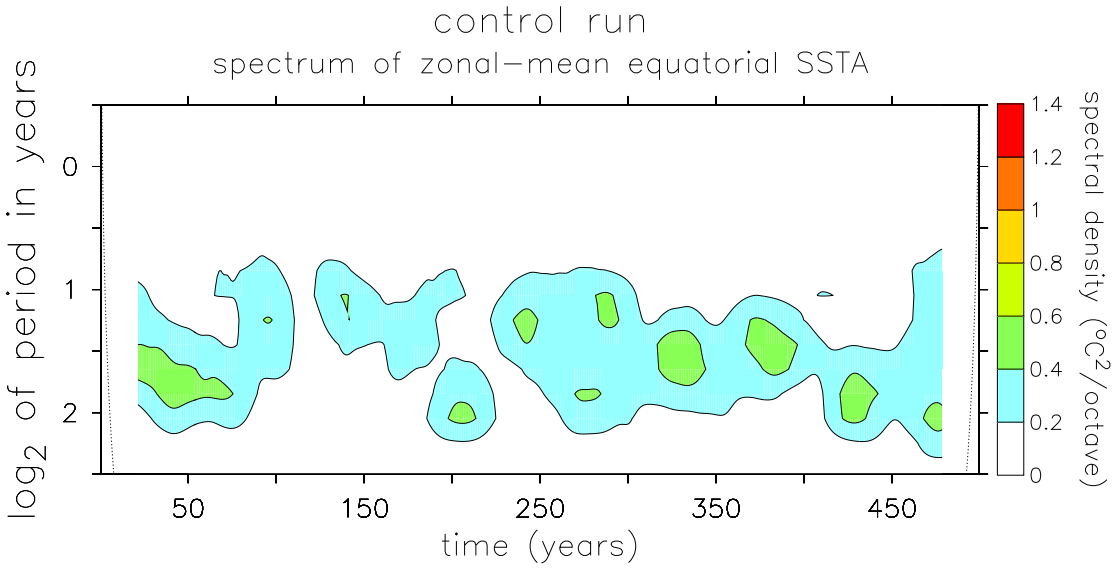

Figure 7.17: Spectral modulation in the stochastic intermediate model control run, based on a wavelet analysis of the unfiltered timeseries shown in Fig. 7.13. Horizontal axis indicates the model time in years. Vertical axis indicates the base-2 logarithm of the period in years. Contours indicate the wavelet power density, which has been smoothed to eliminate modulations at periods shorter than 50 years. Dotted lines indicate the "cone of influence," below which the wavelet power is reduced by zero padding at the beginning and end of the timeseries.

to a fast mode (for strong trades).

7.3.3 Spectrum

Fig. 7.17 shows the "natural" slow variation in the spectrum of zonal-mean equatorial SST anomalies from the stochastic control run. The power in the interannual band varies from century to century, simply due to random fluctuations in the statistically-steady noise. There are also apparent shifts in the dominant period of oscillation: between years 375 and 425, for example, the period shifts from 2.7 to 3.6 years for no reason other than chance. Again, one must be careful to test supposed climate-induced ENSO changes against the hypothesis of stationarity.

To support these tests, we present confidence bands for the control spectrum in Fig. 7.18. The shaded bands indicate the uncertainty that results from trying to characterize the spectrum using short timeseries. The sample spectrum for a 10-year timeseries is extremely variable, suggesting that spectral changes in the interannual band will be difficult to detect at decadal scales. Even for timeseries as long as 250 years, the spectral density in the interannual band can vary by nearly a factor of two. It is important to note, however, that away from the spectral peak the confidence bands narrow substantially. This suggests that it may be relatively easy to detect a *shift* in the spectrum towards longer or shorter periods, which would increase variability in bands that are inactive in the control run.

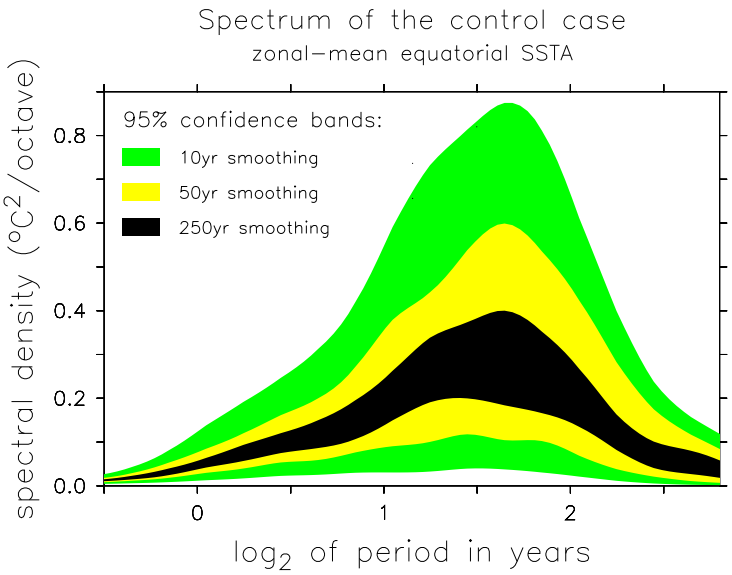

Figure 7.18: Wavelet power spectral density of zonal-mean equatorial (2°S–2°N) SST anomalies, based on the control run of the stochastic coupled intermediate model. Horizontal axis indicates the base-2 logarithm of the period in years. The shaded bands are 95% confidence intervals for the spectrum, based on a 5000 year simulation smoothed to eliminate modulations at periods shorter than 10 years (green), 50 years (yellow), and 250 years (black). Thus the green band indicates that on time scales longer than 10 years, to 95% confidence the spectral density at 2 years will lie between 0.03 and 0.55°C^2/octave.

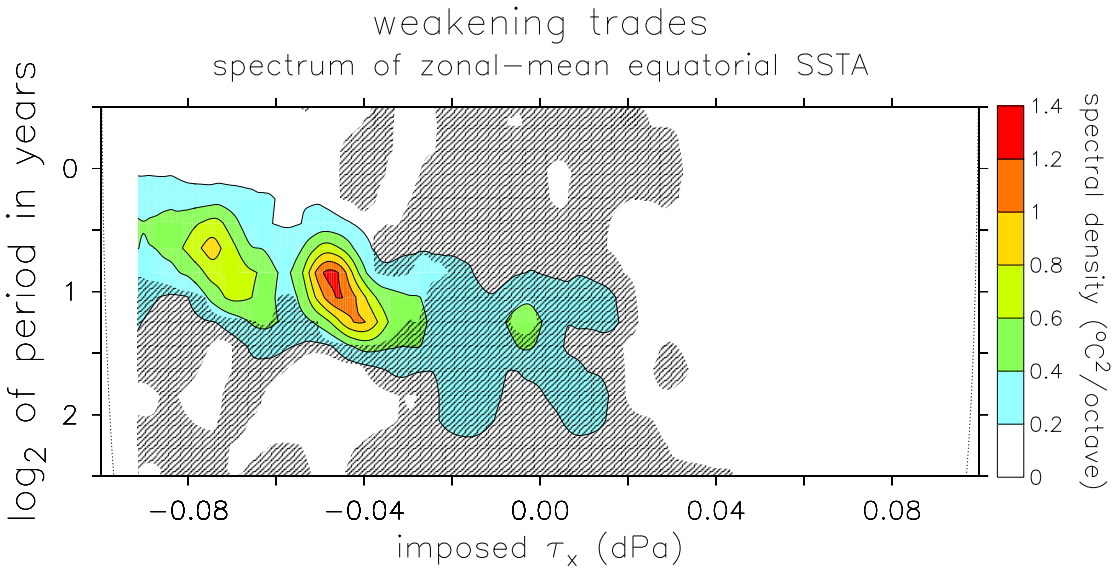

Figure 7.19: Spectral response of the stochastic intermediate model to a weakening of the equatorial trade winds, based on a wavelet analysis of the unfiltered 500-year timeseries shown in Fig. 7.14. Hatching indicates regions that are within the 95% confidence bounds for the 50-year smoothed density in a very long (5000-year) control run. Otherwise as in Fig. 7.17.

How does the period of the stochastic ENSO change as climate changes? Fig. 7.19 shows that as the equatorial trades winds weaken, the ENSO period tends to increase as expected from Sections 7.1 and 7.2. Note that this spectrum is directly comparable to Fig. 7.17 since it is driven by the same realization of the wind stress noise; this is why the two spectra look similar when the imposed zonal stress is near zero. The apparent "resonances" that arise near $\widetilde{\overline{\tau}_x^*} = -0.07$ dPa and $\widetilde{\overline{\tau}_x^*} = -0.05$ dPa, and the apparent "anti-resonance" at $\widetilde{\overline{\tau}_x^*} = -0.06$ dPa, are likely due to chance variations in the stochastic forcing since similar features are found at these times in the control run.

On timescales of 50 years or longer, these spectral changes are robust enough to be distinguished from natural variability. For strong trades ($\widetilde{\overline{\tau}_x^*} \le -0.03$ dPa), short periods are significantly *more* active than in the control, while for weak trades ($\widetilde{\overline{\tau}_x^*} \ge 0.03$ dPa), all periods are significantly *less* active than in the control. Note that at periods of about 3 years, where the control run is most active, the spectral effect of strengthening trades is undetectable even with 50-year timeseries. Instead, the ENSO fingerprint of climate change most clearly revealed in the increased variability in the 1–2 year band, which was relatively inactive in the control run. The key point is this: perhaps the best place to look for evidence of past and future changes is not in the spectral band where ENSO is most active today, but instead at the shorter and longer timescales that are now relatively quiet. These "edge bands" may well be the most sensitive to climate changes that induce shifts in the spectrum.

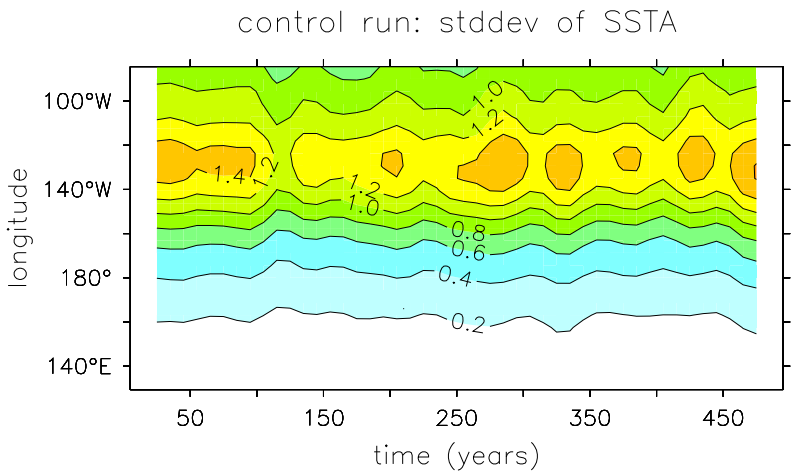

Figure 7.20: Running standard deviation of SST anomalies along the equator (2°S–2°N) in the control run of the stochastic intermediate model. Horizontal axis is the model time in years, vertical axis is longitude. Contours indicate the standard deviation, computed by high-pass filtering the SSTA to eliminate periods longer than 8 years, squaring the result, low-pass filtering to eliminate periods shorter than 50 years, and then taking the square root.

7.3.4 Spatial structure

Fig. 7.20 shows the random modulation of the equatorial SST variability in the control run. While there are variations in the ENSO amplitude as noted earlier, the zonal structure of the variability is rather fixed in time, with a peak amplitude near 130°W and little variability in the western Pacific. Confidence bands for the standard deviation are given in Fig. 7.18.

How does the equatorial structure of ENSO change as climate changes? Fig. 7.22 shows that as the climatological trades weaken, the SST variability shifts eastward, again as expected from Sections 7.1 and 7.2. On timescales of 50 years or more, these changes are readily distinguishable from the stochastic control run. For strong trades ($\widetilde{\overline{\tau}_x^*} \le -0.02$ dPa), the SSTA variability is significantly stronger than the control in the western and central Pacific, and significantly weaker in the far eastern Pacific. For weak trades ($\widetilde{\overline{\tau}_x^*} \ge 0.02$ dPa), the variability is significantly weaker than the control, everywhere along the equator except in the far western Pacific. Again, the implication for ENSO-change studies is that the best place to look for the influence of climate may not where ENSO is most active today, but instead farther west, at the edge of the present variability, where paleodata are likely to be most sensitive to climate-induced zonal shifts in ENSO over time.

7.3.5 Predictability

Given that the distribution, spectrum, and structure of ENSO are all significantly affected by changes in the climatology, is ENSO predictability affected as well? Again, we must first appreciate the natural stochastic variations in predictability. Fig. 7.23 shows

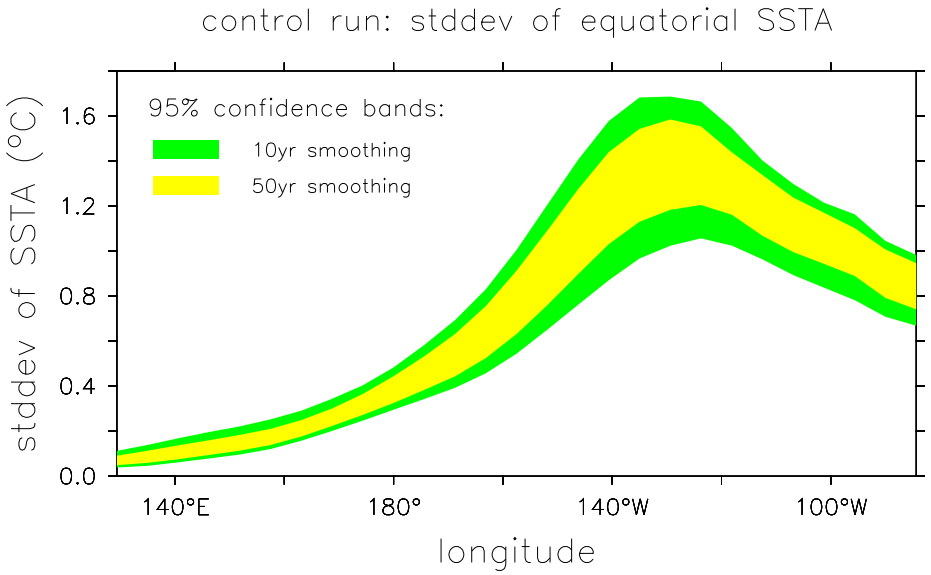

Figure 7.21: Confidence bands for the running standard deviation of SST anomalies along the equator (2°S–2°N) in the control run of the stochastic intermediate model. The standard deviation is computed by high-pass filtering the SSTA to eliminate periods longer than 8 years, squaring the result, low-pass filtering, and then taking the square root. The shaded bands are 95% confidence intervals for the standard deviation for a low-pass filter that eliminates periods shorter than 10 years (green) or 50 years (yellow).

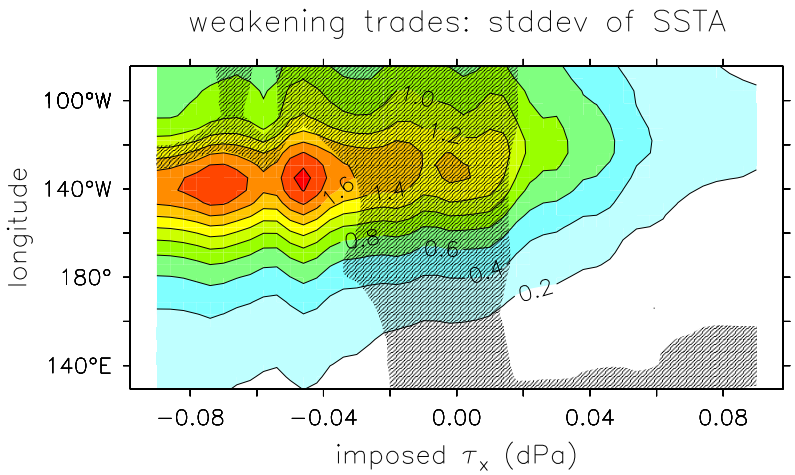

Figure 7.22: Running standard deviation of equatorial SSTA as the equatorial trade winds gradually weaken. Horizontal axis indicates the amplitude of the imposed stress; otherwise as in Fig. 7.20. Hatching indicates regions that are within the 95% confidence bounds for the standard deviation in the control run.

how the predictive power (PP) of the control-run ENSO varies over long time scales, due to the stochastic excitation. The predictive power of a large ensemble does not appear to fluctuate much at time scales longer than 50 years, at least not for those early lead times where the PP significantly greater than zero, and the window of significant predictability generally lasts about 7–10 months. Confidence bands for the smoothed PP are shown in Fig. 7.24.

How does the predictability of ENSO then change as climate changes? Fig. 7.25 shows that as the climatological trades weaken, the predictability window begins to close. This is consistent with Figs. 7.10–7.12, which showed that as the climatological trades weaken, the SSTA response to a wind stress kick becomes more transient—i.e. it dissipates initial information more rapidly. For strong trades, forecasts yield useful information for a full year after initialization, but for weak trades the forecasts become useless after only three months. Fortunately, the predictability appears to be greatest when the ENSO signal is strong, which is presumably the regime where one most depends on forecasts.

These changes are readily distinguishable from the control run, if one examines the average predictability over periods longer than 50 years. For strong trades ($\widetilde{\tau_x^*} \leq -0.02$ dPa), the PP is significantly enhanced at forecast leads of 5–12 months. For weak trades ($\widetilde{\tau_x^*} \geq 0.01$ dPa), the PP is significantly reduced at all leads where the forecasts are useful.

7.3.6 Summary

In the stochastic regime, the effect of climate perturbations on ENSO appears to be similar to that in the absence of noise (Sections 7.1 and 7.2). Compared to the control run, experiments with weakened trades exhibit an ENSO that is weaker, more skewed towards La Niña, and less predictable, with a longer period and an SSTA pattern that is shifted eastward. Experiments with strengthened trades, on the other hand, show an ENSO that is more skewed towards El Niño and more predictable, with a shorter period and an SSTA pattern that is shifted westward.

Whether these changes can be detected in the stochastic context depends on two things: the magnitude of the climate change and the duration of the timeseries. Nearly all of the ENSO changes described above are detectable in 50-year timeseries given an imposed 0.04 dPa change in equatorial zonal-mean stress. This is roughly 30–40% of the standard deviation of interannual zonal stress anomalies observed over the past few decades (Fig. 2.5a), and is the same order of magnitude as the change observed between 1960-79 and 1980–99 (Fig. 2.1a). This suggests that the ENSO variations observed over the past several decades could well be linked to changes in the climatology. The results in this section further suggest that these changes should be most detectable at the "edges" of the present-day ENSO variability, where the statistics can most clearly reveal shifts in the distribution, spectrum, and spatial pattern of variability.

Unfortunately, as noted in Chapter 2, the *disparity* between observational analyses is also the same order of magnitude as the climate and ENSO changes we wish to detect. Thus the attribution of ENSO changes to climate changes, while plausible, may be hard to justify without improved analyses or the accumulation of additional data. On the other hand, the large climate differences in the analyses, combined with the discernable effect of climate on ENSO, may be one clue as to why ENSOs differ among coupled GCMs,

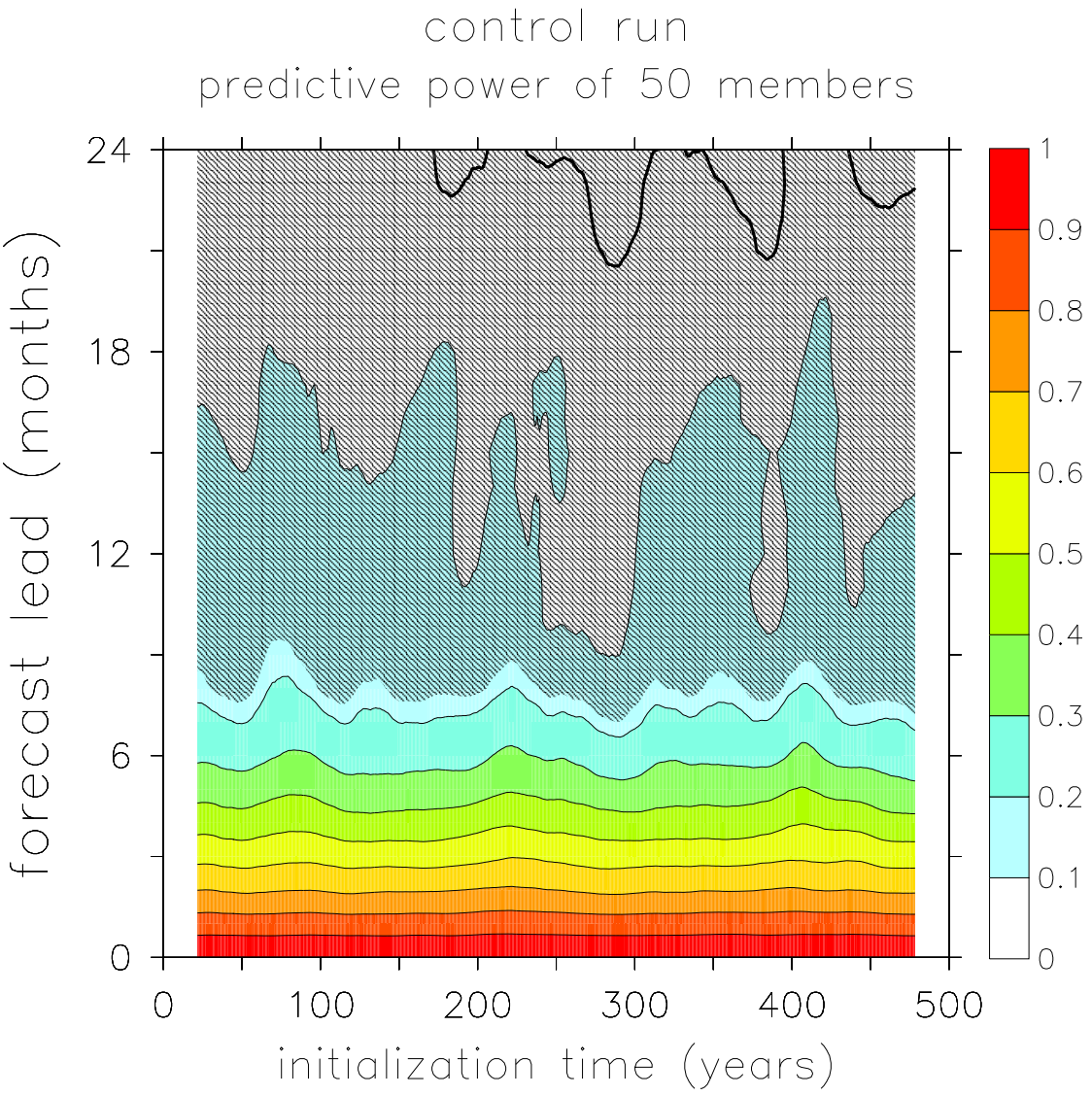

Figure 7.23: Predictive power (PP) of 50 ensemble members, in the control run of the stochastic intermediate model. Horizontal axis is the model initialization time in years. Vertical axis is the forecast lead time. Contours indicate the PP, which has been smoothed in time to eliminate amplitude modulations at periods shorter than 50 years. Hatching indicates regions of insignificant PP, where the probability of positive PP is less than 95%.

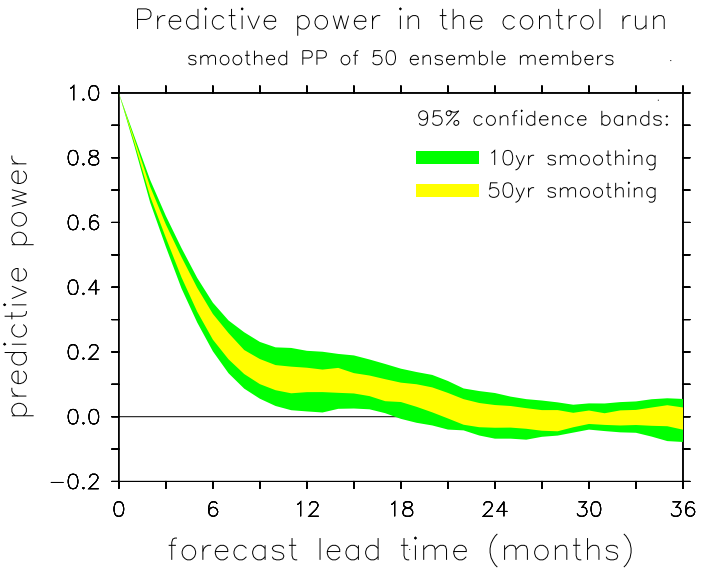

Figure 7.24: Smoothed predictive power (PP) of zonal-mean equatorial (2°S–2°N) SST anomalies in the control run of the stochastic intermediate model. The shaded bands are 95% confidence intervals for PP smoothed by a low-pass filter that eliminates PP variations at periods shorter than 10 years (green) or 50 years (yellow).

and between the models and observations. Uncoupled atmosphere or ocean GCMs, forced by erroneous analyses and tuned to reproduce erroneous analyses, may drift toward an erroneous climate when coupled and thereby alter the simulated ENSO.

7.4 Hybrid coupled GCM experiments

Having found a significant impact of the background state on ENSO in the intermediate model, we now ask: Does a coupled GCM exhibit similar sensitivity?

7.4.1 Design of the experiments

To answer this question, we turn to a hybrid coupled model consisting of an ocean GCM coupled to a statistical atmosphere (Appendix F). Compared to the intermediate model, the ocean GCM is a much more sophisticated treatment of ocean dynamics and mixing, with full nonlinearity and a seasonally-varying background state. The statistical atmosphere in this case includes a nonlocal representation of both the wind stress and the surface heat fluxes, but supports only a single degree of freedom and so cannot represent propagating features or changes in the stress anomaly patterns.

The hybrid GCM is roughly 10,000 times more expensive to run than the intermediate model, so we must choose our experiments carefully. Fortunately, the intermediate model results offer useful guidance in this regard. Based on Section 7.1, the climate parameter of greatest interest appears to be the strength of the equatorial zonal stress, which can

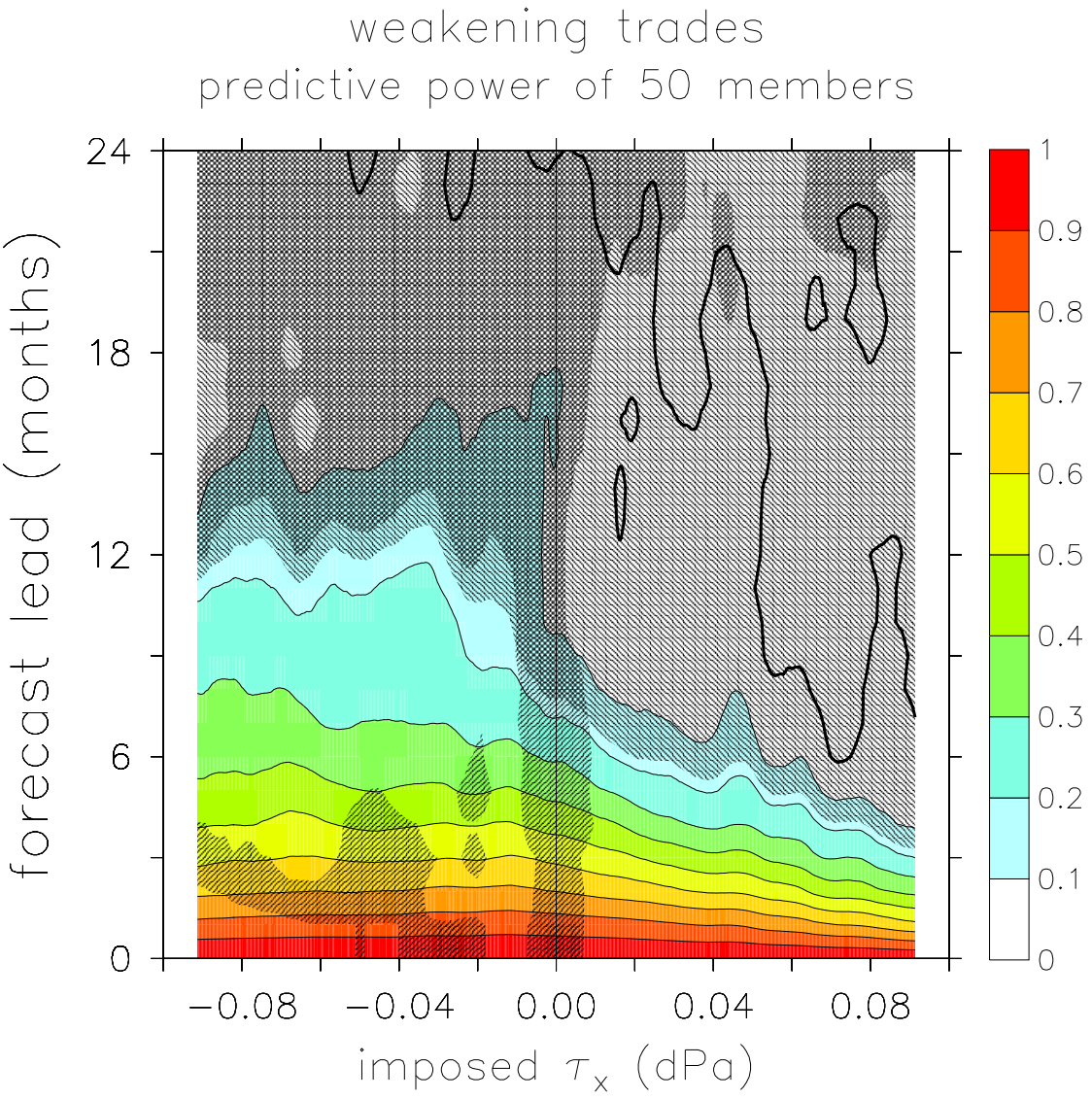

Figure 7.25: Predictive power as the equatorial trade winds gradually weaken. Horizontal axis indicates the amplitude of the imposed zonal stress. Hatching that ramps up to the right indicates regions that are within the 95% confidence bounds for PP in the control run. Otherwise as in Fig. 7.23.

stand in for a wide range of possible climate changes as far as ENSO is concerned. Second, from Section 7.3 it appears that many of the ENSO changes observed in the most realistic stochastic regime tend to be evident even when no noise is present, so we can forgo long stochastic runs in the HGCM.

Thus we perform two perturbation experiments, subjecting the HGCM to a zonal wind stress perturbation which is constant in time and has the spatial form (5.3) with $L_x = 40°$, $L_y = 15°$, and an equatorial maximum of $\widetilde{\tau_x^*} = \pm 0.1$ dPa at longitude $x_0 = 140°$W. The GCM is spun up for 4 years, and the subsequent 16 years are used to compute a monthly climatology that is subtracted from the total fields to yield monthly anomalies. (The climatologies for these experiments were described in Chapter 5.) Advection terms are computed on the model grid from the monthly-mean climatology and anomalies, and then averaged over the top 50 m of the ocean. Subtracting the vertically-averaged total advection and surface heat flux terms from the total temperature tendency then gives a residual heating, which is assumed to arise from high-frequency mixing. Finally, the advection, surface flux, and mixing fields are averaged onto a coarse (2° lat × 5.625° lon) grid for ease of comparison with the intermediate model.

7.4.2 Overview of the equatorial-trades prototype

Equatorial SST anomalies

Fig. 7.26 shows the equatorial evolution of SST anomalies in the control and perturbed HGCM cases, beginning four years after initialization. The control exhibits a sustained oscillation with a period of about 3.3 years, a peak-to-peak NINO3 SSTA amplitude of about 2.3°C, and westward propagation of SST anomalies in the central Pacific. For strengthened trades, the model ENSO is damped and has a slightly shorter period of 3.1 years. For weakened trades, the HGCM exhibits a sustained series of long warm events punctuated every 5.5 years by short, strong cold events, which is very similar to the behavior of the intermediate model at high coupling (Fig. 7.27).

Heat budget phasors

What is responsible for these changes in behavior? The phasor diagrams in Fig. 7.26 indicate the relative roles of advection, surface heat fluxes, and mixing in the evolution of zonal-mean SST anomalies in the hybrid coupled GCM. The diagrams are prepared as in Section 7.1.2, except that here "m" refers to the background state of the altered model climatology (as opposed to the control climatology), and "p" refers to perturbations from this altered background state. Thus changes in the "uptm" term, for example, represent changes in both the mean SST gradient and the anomalous zonal current variability.

In the control case, the primary terms affecting the temperature of the top 50 m of the ocean are the surface flux, $-\overline{w}\partial_z T'$, and $-u'\partial_x \overline{T}$. The surface flux provides a strong damping, which lags the SSTA slightly and so facilitates the transition between warm and cold phases. The $-\overline{w}\partial_z T'$ term is largely responsible for maintaining the oscillation amplitude in the face of damping by the surface flux. The $-u'\partial_x \overline{T}$ term, which is nearly in quadrature with SSTA, plays a strong transitioning role and is the largest factor in determining the oscillation period.

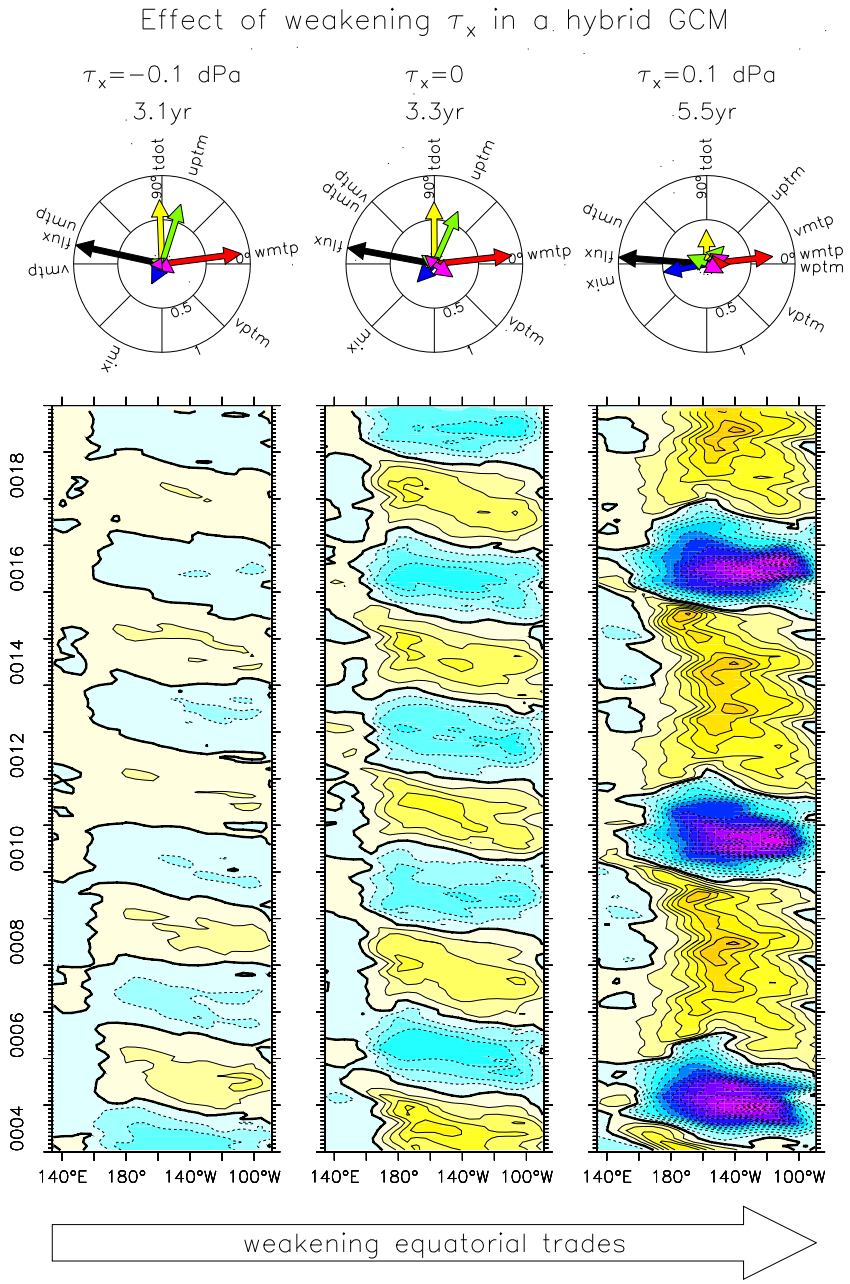

Figure 7.26: Change in ENSO due to a change in mean trade winds, as simulated by a hybrid coupled GCM. Time-longitude plots (bottom row) show the equatorial (2°S–2°N) evolution of SST anomalies, for a period of 16 years beginning four years after initialization. Contour interval is 0.5°C, with a thick line at 0°C; warm (cool) colors indicate positive (negative) anomalies. Labels at top indicate the amplitude of the imposed climate perturbation (the trades winds weaken to the right) and the oscillation period. Phasors (middle row) show the amplitude (relative to surface heat flux) and phase lead (relative to local SSTA) of the temperature tendency terms, averaged zonally across the basin in the equatorial band.

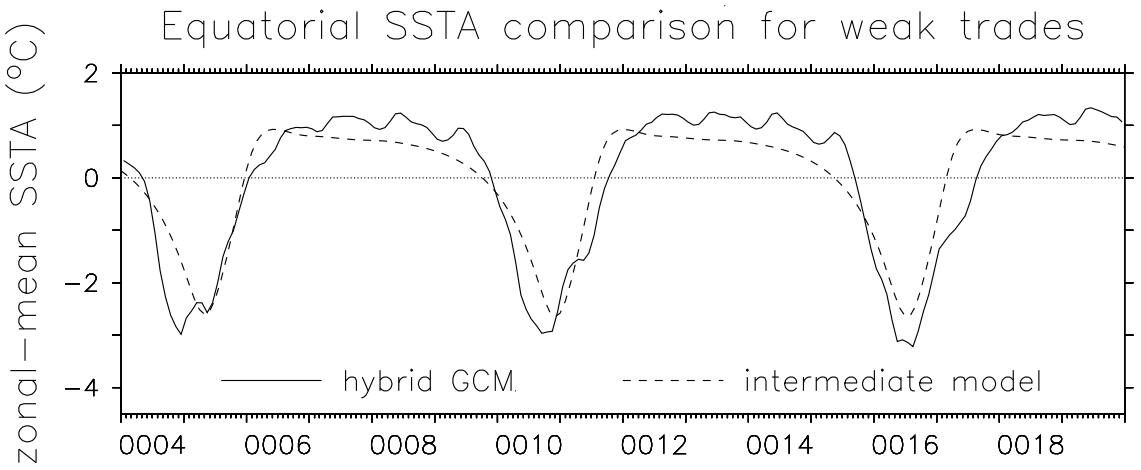

Figure 7.27: Comparison of zonal-mean equatorial (2°S–2°N) SST anomalies from two models. Solid line corresponds to the GCM weak-trades case; dashed line corresponds to the intermediate model with $\mu = 1.2$ and imposed zonally-constant westerly stress with peak amplitude 0.011 dPa at the equator. Horizontal axis indicates years since initialization.

In the strong-trades case, the zonal-mean heat budget is only subtly changed from the control case. A slight weakening of $-v'\partial_y\overline{T}$ reduces the coupled instability relative to the control, and is responsible for the gradual damping of the oscillation. The weakening of $-v'\partial_y\overline{T}$ also reduces its anti-transitioning effect, which along with the strengthening of $-u'\partial_x\overline{T}$ and the increased phase lead of $-\overline{w}\partial_z T'$ ahead of SSTA, is responsible for the slightly shorter period relative to the control case.

The weak-trades case, on the other hand, differs markedly from the control. The weakening of the climatological cold tongue in the east greatly reduces the transitioning role of zonal advection during warm events, which contributes to the lengthening of the oscillation period. Both $-w'\partial_z\overline{T}$ and $-\overline{v}\partial_y T'$ become important destabilizers, opposing the damping of equatorial SSTAs by mixing and $-\overline{u}\partial_x T'$. It is clear from the skewness of the oscillation that nonlinearities are playing a key role in this case.

7.4.3 Evolution of the equatorial vertical structure

What is going on below the surface to cause these changes in the mechanism and behavior of the HGCM ENSO? In this section we examine vertical slices of the simulated equatorial fields along the equator, exactly as in the intermediate model case. We will show that there are several key differences between the models in how the equatorial structure of ENSO responds to changes in the climatology.

Control run

Fig. 7.28 shows equatorial snapshots from the HGCM control run, at 3-month intervals beginning in January of year 7. The story begins with anomalous eastward currents and an anomalously deep thermocline all along the equator. Eastward advection of the warm pool

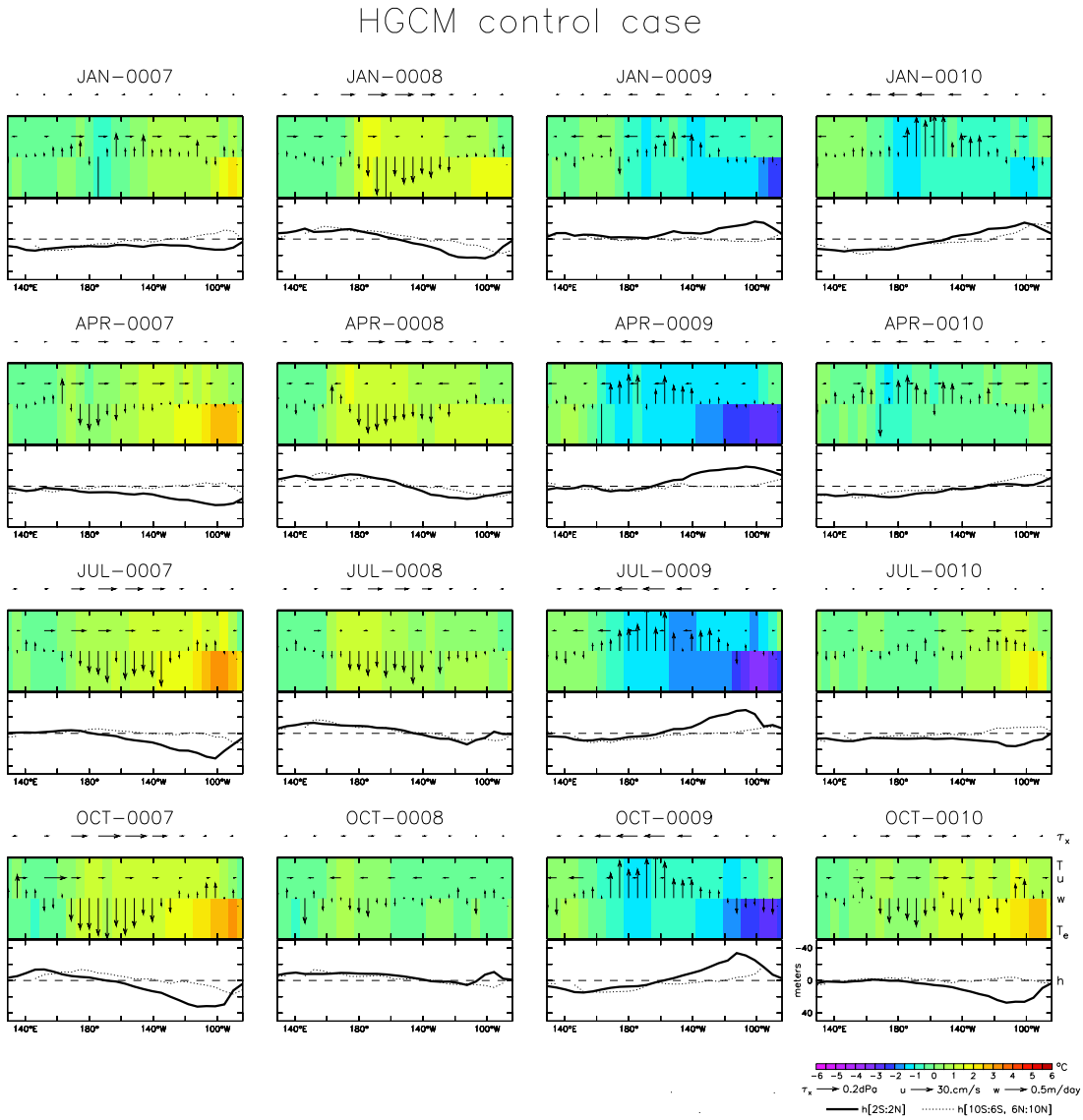

Figure 7.28: Equatorial snapshots at three-month intervals from the HGCM control case. Time flows down each column then left to right. Bottom right panel gives contour/vector keys for all panels. Vectors indicate anomalies of (top to bottom) zonal surface stress, average zonal velocity of the top 50 m of the ocean, and upwelling velocity at 50 m depth. Shading indicates the anomalous temperature in the well-mixed surface layer (top) and at 50 m depth (bottom). Bottom subpanel shows the anomalous depth of the 20°C isotherm (ordinate reversed), at the equator (2°S–2°N, solid) and off-equator (6–10° N/S, dotted).

and warmer entrainment into the mixed layer leads to a warming of the central and eastern Pacific, which then incites westerly stress anomalies over the central basin. These stress anomalies induce anomalous downwelling in the central basin and enhance the deepening of the thermocline in the east, completing a positive feedback loop that launches the system into a warm event.

Meanwhile, the thermocline begins to shoal in the west and off-equator in October of year 7, as upwelling Rossby signals arrive from the region of anomalous stress forcing. Gradually, this off-equatorial shoaling draws heat content from the equatorial waveguide along the western boundary. A reversal of the equatorial current anomalies begins in the eastern Pacific around January of year 8, and then spreads westward, cooling the surface and weakening the westerly stress anomalies. This reduces the thermocline slope and shoals the thermocline in the east, so that cooler water is entrained into the eastern Pacific mixed layer (October of year 8). As the westward current anomalies and shallow thermocline continue to cool the mixed layer past the climatological equilibrium, the system is propelled into a cold event, which then evolves in the opposite sense as the warm event.

Thus ENSO in the HGCM control run appears to be largely of the "recharge" or "delayed oscillator" type, with a period set by slow ocean adjustment via internal waves. Elements of "SST mode" behavior are also evident, such as in the westward-propagating SST anomalies which lag behind similarly-propagating the zonal current anomalies. The control ENSO is thus a hybrid mode, with meridional recharge providing the "overshoot" necessary to initiate events, but with coupled surface dynamics determining the subsequent spatial structure and propagation of the anomalies.

Several differences are evident between the HGCM ENSO and that in the intermediate model. The HGCM does not exhibit coherent westward propagation of off-equatorial thermocline depth anomalies, presumably due to the downward propagation of Rossby waves emerging from the eastern boundary. The thermocline depth anomalies in the western Pacific are also weaker in the HGCM, since in nonlinear balance the deep warm layer in the west requires less of a surface slope to balance the wind stress than does a linear active-layer model (Section 4.2.1). In the western and central Pacific, the HGCM temperature anomaly at 50 m generally tracks closely to the SST anomaly due to the deep mixed layer there; the intermediate model, in contrast, often showed substantial differences developing between T_e' and T' in the west, which led to overly strong SSTA-damping due to mean upwelling.

Case with strong mean trades

The GCM case with strengthened trades evolves in a manner so similar to the control run that scaled equatorial snapshots for the two cases look nearly identical. We therefore postpone discussion of this case to Section 7.4.4.

Case with weak mean trades

Fig. 7.29 shows equatorial snapshots from the hybrid GCM case with weakened trades, beginning in January of year 6. The warm event is sustained for nearly 3.5 years, during which time there are strong equatorial westerly stress anomalies, downwelling anomalies,

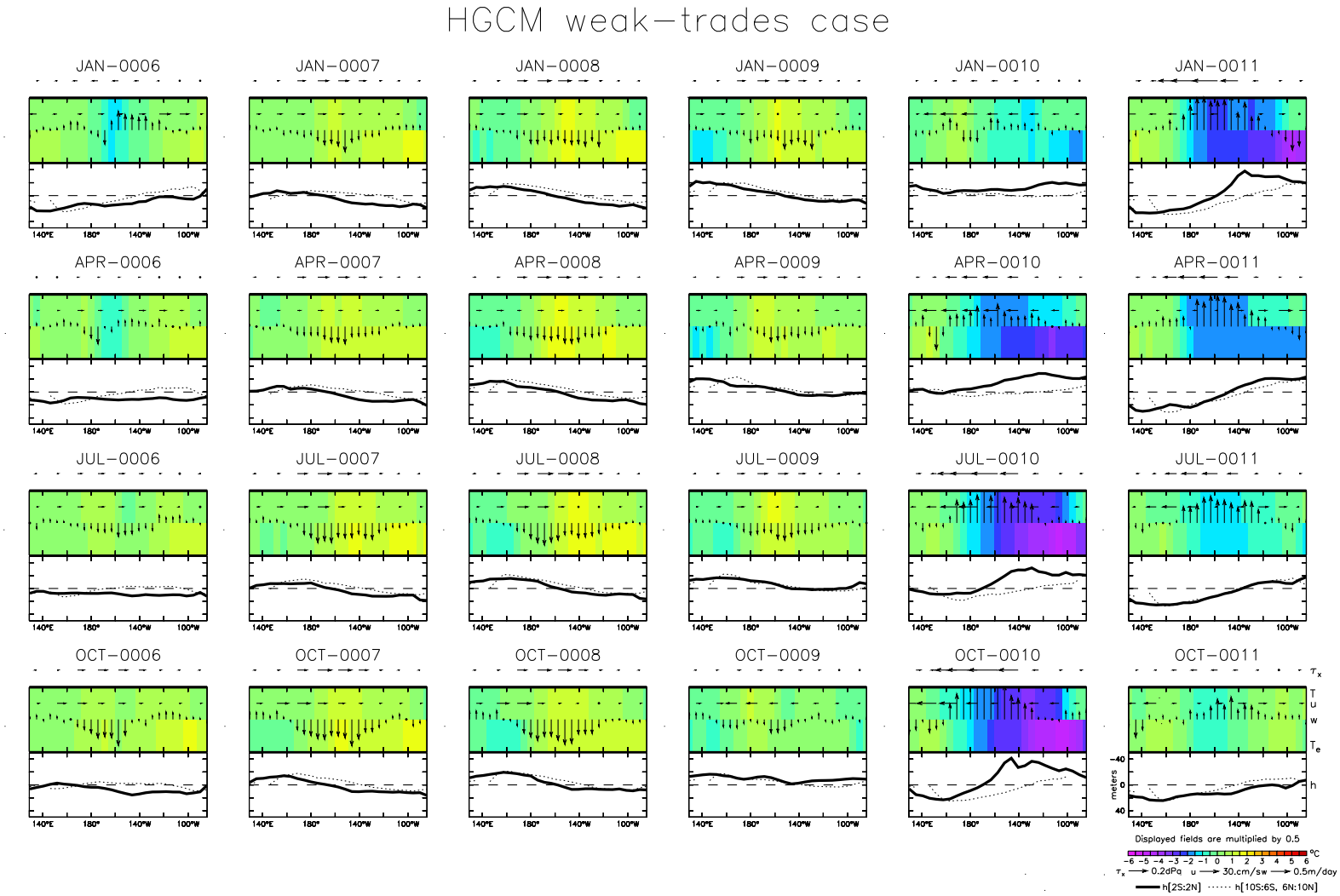

Figure 7.29: Equatorial snapshots at three-month intervals from the HGCM case with weakened trades ($\widetilde{\overline{\tau}^*_x} = 0.1$ dPa). Otherwise as in Fig. 7.28.

and eastward current anomalies in the central Pacific, and a deepened thermocline in the east. An east-west sloshing of the SST anomalies is also apparent during the warm event, as the SSTAs are advected by the seasonally-varying mixed-layer currents, which are eastward in boreal spring and early summer but westward the rest of the year.

The continued presence of westerly stress anomalies slowly generates a sizable shoaling of the off-equatorial thermocline in west, which gradually drains heat content from the equatorial band along the western boundary. This can have only a limited effect the SST anomaly, however, since total upwelling is nearly shut off and there is only a weak zonal SST gradient upon which the zonal current anomalies can act. The warm event is thus prolonged, decaying slowly via surface fluxes, until eventually the warm surface temperatures erode and the trade easterlies are reestablished.

As the westerly anomalies weaken, the equatorial zonal current anomalies reverse and the equatorial thermocline shoals in the east (October of year 9), bringing an end to the warm event. The strengthening of the easterly stress ignites an explosive cooling, as fresh upwelling begins to act on an ever-increasing vertical temperature gradient in the east. Meanwhile, the paucity of heat content in the off-equatorial western basin continues to siphon mass out of the equatorial band, further shoaling the equatorial thermocline and enhancing the westward advection of the cold tongue. A combination of strong upwelling, strong westward currents, and a strong shoaling of the thermocline in the east produces a sizable cold event which quickly recharges the heat content in the off-equatorial western Pacific. During these strong cold events, energetic tropical instability waves develop just off-equator, and contribute to the restoration of warm temperatures by stirring in warm off-equatorial water. The cooling peaks as the westward current anomalies weaken (October of year 9), and then terminates as the current anomalies reverse and the thermocline deepens in the east (October of year 11).

Thus nonlinearities appear to play a key role in the HGCM ENSO for weak climatological trades. The disappearance of upwelling and the zonal SST contrast during warm events is important for lengthening the oscillation period, since it delays the surface adjustment to changes in the meridional structure of the thermocline. This delay is also important for generating the strong cold events that quickly recharge the equatorial heat content, since it allows excessive negative heat content anomalies to develop off-equator during warm events.

This nonlinear delay mechanism is more severe than in the weak-trades case of the intermediate model at standard coupling, but it does play a significant role in the latter at higher coupling where the equatorial easterly stress disappears during warm events (Figs.7.9 and 7.27). Such a comparison is probably appropriate, since the intermediate model at "normal" trades can only support sustained oscillations (such as those in the HGCM control run) when the coupling is stronger than the standard value. The nonlinearity responsible for the HGCM cold-skewness at weak trades is also echoed in the stochastic intermediate model at standard coupling, where the SSTA distribution goes from warm-skew to cold-skew as the trades weaken (Fig. 7.16). In a broader sense, the nonlinearity associated with the weakening of the *climatological* zonal SST gradient is even responsible for the increase in the period of the intermediate model ENSO at small amplitudes (Fig. 7.1), since as the climatological trades go from "strong" to "normal" the transitioning effect of $-u'\partial_x\overline{T}$ is

reduced. Thus many elements of the HGCM ENSO response to changes in the equatorial trades actually mirror those found in the intermediate model.

7.4.4 Change in the mixed layer heat budget

What is the quantitative change in the HGCM ENSO mechanism as climate changes, and how is it related to the intermediate model? Fig. 7.30 shows the mixed layer heat budget along the equator for each of the three HGCM cases. As in the intermediate model, the change in the strength of the climatological trades induces substantial changes in the ENSO mechanism along the equator. A glance at Fig. 7.30 shows that these changes are complex and spatially-dependent. We shall consider them one at a time, at four key longitudes along the equator.

110°W

In the far eastern Pacific of the HGCM control run, $-\overline{w}\partial_z T'$ and $-\overline{v}\partial_y T'$ act in concert as destabilizers, maintaining the oscillation amplitude in the face of surface heat fluxes and mixing. Since the destabilizers lag SSTA slightly they delay the transitions between events, which serves to lengthen the ENSO period. The $-u'\partial_x \overline{T}$ term, on the other hand, is nearly in quadrature with local SSTA and thus plays a strong transitioning role. Note that the surface flux and mixing terms are also important transitioners, since the damping associated with them lags SSTA by 20–30°. The $-w'\partial_z \overline{T}$ and $-v'\partial_y \overline{T}$ terms, which are rather weak at 110°W, both act to damp the local oscillation but play opposite roles in the transition.

Some differences from the intermediate model control run (Fig. 7.6) are already evident. In the intermediate model at 110°W, zonal advection and mixing were negligible, and the surface flux played only a damping role, meridional advection was less important, and $-\overline{w}\partial_z T'$ led instead of lagged SSTA. The heat budget in the HGCM is more reminiscent of the intermediate model *strong-trades case* between 110–140°W, which makes sense since the HGCM control run is known to have an overly strong cold tongue at the equator (Fig. F.4h).

In the HGCM strong-trades case, $-\overline{w}\partial_z T'$ plays a larger role, and it along with $-\overline{v}\partial_y T'$ become more purely destabilizing than in the control case. This, together with the slightly stronger $-u'\partial_x \overline{T}$, accelerates the transitioning mechanism and slightly increases the oscillation frequency. The frequency increase is largely opposed by the change in mixing, which strengthens and becomes a slight anti-transitioner. The increased damping of the ENSO oscillation at strong trades results from increased dissipation of equatorial anomalies by mixing, probably related to stronger TIWs associated with the enhanced current shear at strong trades.

In the weak-trades case, $-\overline{w}\partial_z T'$ is weaker and more purely destabilizing than in the control. The $-u'\partial_x \overline{T}$ term also plays less of a transitioning role due to the weakened zonal SST gradient; surprisingly, the strongest transitioning term is now the surface heat flux. The precise period of ENSO again depends on a subtle balance, with significant contributions from mixing (a transitioner) and $-w'\partial_z \overline{T}$ (an anti-transitioner). The reduced

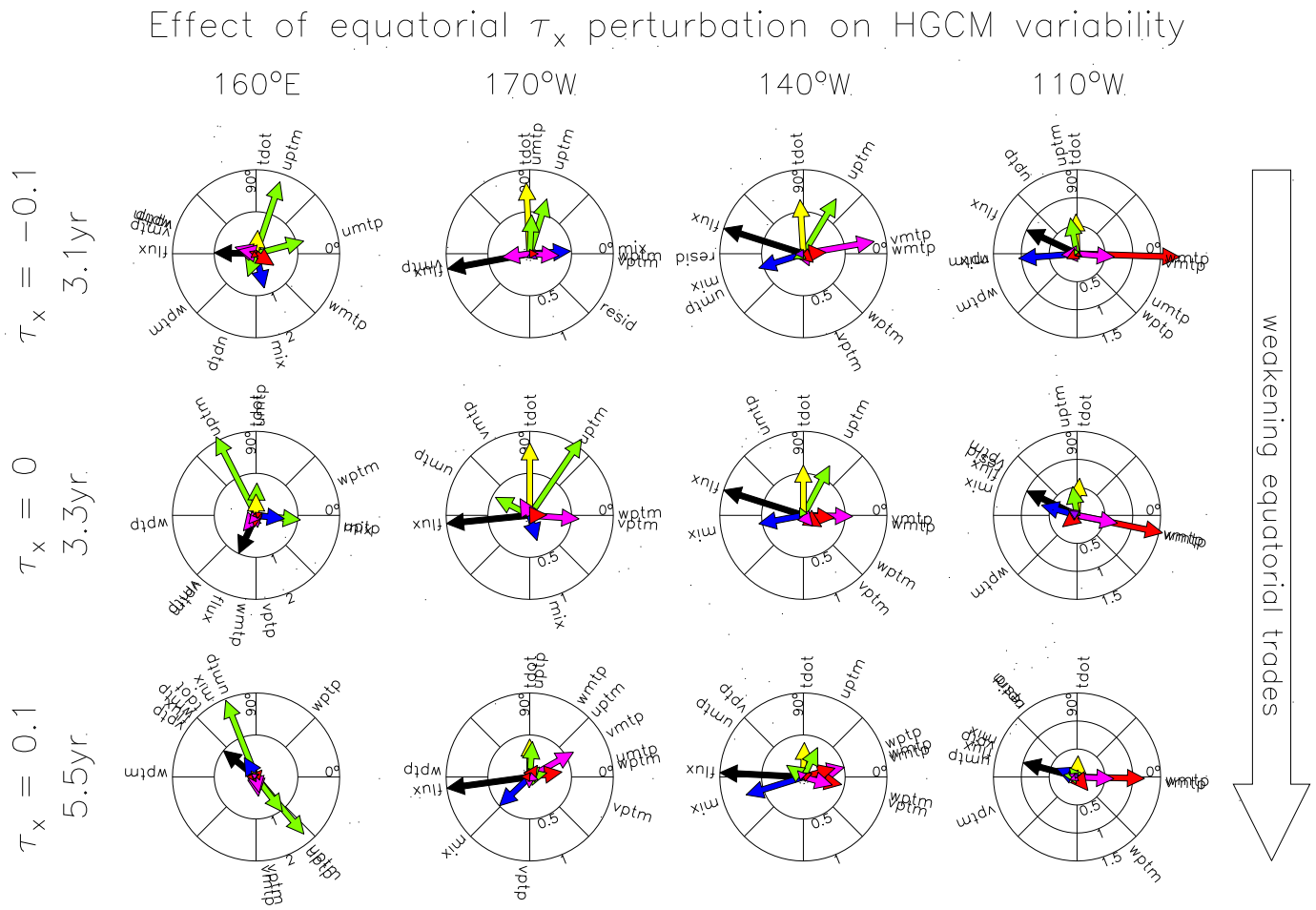

Figure 7.30: Comparison of equatorial mixed layer heat budget phasors for the hybrid GCM cases of Figs. 7.28–7.29. The phasor diagrams are as described in Fig. 7.1 and Section 7.1.2. Middle row is the control case, top row is the case with strengthened trades ($\widetilde{\overline{\tau}^*_x} = -0.1$ dPa), bottom row is the case with weakened trades ($\widetilde{\overline{\tau}^*_x} = 0.1$ dPa). Each column corresponds to a given longitude, progressing from west on the left to east on the right. Diagrams at the same location, i.e. within a given column, have the same scale.

lag of $-w'\partial_z\overline{T}$ behind SSTA has also changed the role of $-w'\partial_z\overline{T}$ from a damper to a destabilizer.

140°W

In the central/eastern Pacific, the HGCM control run shows a smaller role for $-\overline{w}\partial_z T'$ than in the far eastern Pacific. The destabilization is now mostly due to $-\overline{v}\partial_y T'$, with assistance from $-\overline{w}\partial_z T'$, $-u'\partial_x\overline{T}$, $-w'\partial_z\overline{T}$, and $-v'\partial_y\overline{T}$ that balances the damping by the surface fluxes and mixing. The $-u'\partial_x\overline{T}$ term plays a more active role in the transition than it did farther east, which along with the surface flux acts to balance the now anti-transitioning effect of the mixing.

For strong trades, the strong meridional asymmetry of the cold tongue enhances $-\overline{v}\partial_y T'$, which is not only the top destabilizer at 140°W but is also an important transitioner. The $-u'\partial_x\overline{T}$ term is also stronger than in the control, which helps to shorten the oscillation period slightly. There is little change in the roles of the surface fluxes and mixing relative to the control, so the damping of ENSO in the strong-trades case appears to result from more subtle changes, including reduced $-\overline{w}\partial_z T'$ and increased $-\overline{u}\partial_x T'$.

The heat budget of the weak-trades case is even more complex. The $-\overline{w}\partial_z T'$, $-\overline{v}\partial_y T'$, $-w'\partial_z\overline{T}$, and $-v'\partial_y\overline{T}$ terms have roughly the same magnitude and all contribute to the destabilization. The $-u'\partial_x\overline{T}$ term is weaker relative to the surface flux than in the control, though it is still the dominant transitioner at 140°W. The increased period in this case is mainly due to the weakening of the $-u'\partial_x\overline{T}$ transitioner, a reduction in the phase lag of the surface flux damping, and to stronger mixing (which has an anti-transitioning effect). The $-\overline{u}\partial_x T'$ term also enters as an important local damper and transitioner at 140°W, as temperature anomalies are advected slowly westward by the mean currents.

170°W

In the western/central Pacific, the HGCM control run has both a strong climatological westward SST gradient and strong interannual zonal current variations, so there is a stronger role for $-u'\partial_x\overline{T}$ than further east. This term is by far the most important transitioner, and is even the most important destabilizer (slightly ahead of $-v'\partial_y\overline{T}$). The $-\overline{u}\partial_x T'$ and $-\overline{v}\partial_y T'$ terms also appear as damping/transitioning terms. Note that the surface flux and mixing have taken on stronger anti-transitioning roles at this longitude. The $-\overline{w}\partial_z T'$ term no longer plays a role, since at this longitude the thermocline depth does not fluctuate much, and the thermocline is so deep that it has little influence on the temperature of water entrained into the mixed layer.

In the strong-trades case, $-u'\partial_x\overline{T}$ is weaker and plays a more purely transitioning role than in the control run. The only other significant transitioner is $-\overline{u}\partial_x T'$, which also more of a transitioner than it was in the control case. The effect of mixing is stronger than in the control, due to stronger temperature gradients and stronger TIWs in the strong-trades case. Since increased mixing during cold events imports cold water from farther east, mixing acts as a destabilizer at 170°W, which assists $-v'\partial_y\overline{T}$ in the face of damping by $-\overline{v}\partial_y T'$ and strong surface fluxes.

In the weak-trades case, $-u'\partial_x\overline{T}$ is much weaker than in the control. For weak trades, zonal advection occurs almost exclusively during the transitions into cold events, when a strong westward SST gradient appears at 170°W; the rest of the time the zonal SST gradient is very weak at this longitude. This nonlinearity is evident in the large role for $-u'\partial_x T'$, which is nearly identical to the total temperature tendency (since the remaining terms, though large, almost cancel). Nonlinearity is thus very important to the oscillation in the weak-trades case. The transition at this longitude is assisted by $-\overline{v}\partial_y T'$ and opposed by mixing and surface fluxes. The $-w'\partial_z\overline{T}$ term plays a significant role as a destabilizer, and a host of other terms ($-\overline{u}\partial_x T'$, $-\overline{w}\partial_z T'$, $-v'\partial_y T'$) also contribute to the destabilization and transition at 170°W.

160°E

In the western Pacific, the HGCM control run once again shows a large transitioning role for $-u'\partial_x\overline{T}$. In contrast to further east, however, $-u'\partial_x\overline{T}$ also acts as a damper since it leads local SSTAs by more than 90°. In this case the damping by $-u'\partial_x\overline{T}$ is even stronger than that due to the surface heat flux, which has now taken on more of an anti-transitioning role along with meridional and vertical advection. Other zonal advective terms also contribute to the oscillation: $-\overline{u}\partial_x T'$ is a transitioner while $-u'\partial_x T'$ is a destabilizer. Mixing also contributes to local growth by importing anomalous SSTAs from farther east. Thus the total SSTA tendency in the western Pacific of the control run is but a small residual of many large terms that nearly balance.

In the strong-trades case, $-u'\partial_x\overline{T}$ is more of a destabilizer at 160°E than in the control. The $-u'\partial_x T'$ term also plays a different role than in the control run, acting as an anti-transitioner which opposes $-u'\partial_x\overline{T}$ to a small extent. The $-\overline{u}\partial_x T'$ term contributes slightly to the transition, but in contrast to the control plays a much larger role as a destabilizer. The $-\overline{w}\partial_z T'$ term has a dual destabilizing/anti-transitioning effect which is essentially canceled by meridional advection. Mixing is an anti-transitioner, again in contrast to the control run where it was a destabilizer.

In the weak-trades case, the SSTA hardly varies at all at 160°E, except during La Niñas when cold water encroaches from the east. This balance results from a near-perfect cancellation between $-u'\partial_x\overline{T}$, $-u'\partial_x T'$, $-v'\partial_y\overline{T}$, and $-\overline{v}\partial_y T'$ on the one hand (which act as destabilizers and anti-transitioners), and $-\overline{u}\partial_x T'$, surface flux, and mixing on the other hand (which act as stabilizers and transitioners). Note that the role of the surface flux in this case is very different from in the control run.

Heat budget summary

There are several general points to take from Fig. 7.30. The mixed layer heat budget in the hybrid coupled GCM is even more complex than in the intermediate model, with significant contributions from surface heat fluxes, mixing, and full three-dimensional advection everywhere along the equator. The surface fluxes and mixing, in particular, are first-order terms and both show substantial phase changes relative to SSTA at different longitudes and between the control and perturbed-trades cases. This is in contrast to the intermediate model, which assumes simply that surface fluxes act as a linear damping of

local SSTAs. The contribution of fluxes and mixing to the ENSO frequency in the HGCM illustrates the complexity of modeling ENSO, since both of these processes involve highly nonlinear and small-scale variability that is heavily parameterized in the current generation of coupled GCMs. This may be yet another reason why different models simulate such different ENSOs, and why they often show poor agreement with observations.

In the HGCM, the strong-trades case evolves in much the same way as the control run, and its heat budget closely mirrors that of the control, apart from a larger role for zonal advection in the east and a more complex array of differences in the western/central Pacific. The weak-trades case is very different from the control, with a decreased role for zonal advection and with nonlinearities playing a key role in determining the oscillation period and skewness.

7.5 Chapter summary and discussion

This chapter has examined the sensitivity of ENSO to changes in the climatological background state, using a hierarchy of ocean-atmosphere models. In the simplest case, an intermediate model is perturbed slightly and then allowed to evolve under the influence of climatological trades of varying strengths. The results show that as the trades weaken, the oscillation period increases and the pattern of SST anomalies shifts eastward. Oscillations are rapidly damped when the trades are weak, but are less damped at intermediate and strong trades. For weak trades, a weakened zonal SST gradient inhibits the transitioning effect of zonal advection, and the increased depth of the thermocline in the east inhibits the growth of SST anomalies by desensitizing the entrainment temperature to vertical motions of the thermocline. For strong trades, the increased zonal SST gradient enhances the transitioning effect of zonal advection, while the outcropping of the thermocline in the east causes the SST variability to shift westward into the central basin. Similar results are found for other types of climate perturbations, whose primary effect is to set into motion coupled feedbacks that set the climatological strength of the equatorial trades.

The climate-induced changes of stability and period in the intermediate model are echoed in the nonlinear regime. As the air-sea coupling increases, a sustained ENSO appears first at intermediate and strong trades, just where control case showed the weakest damping of ENSO in response to small kicks; and as in the control run, the period of the sustained ENSO lengthens as the trades weaken. For strong wind stress kicks, a new wrinkle is added by short-term transients, which are strong relative to the subsequent modal oscillations and are heavily influenced by nonlinearity. The transients too are affected by the climatology, but they bear little direct relation to the properties of the least-damped mode.

In the stochastic regime, too, climate has a significant impact on ENSO: As the trades weaken, ENSO shifts to longer periods, weaker amplitudes, and farther east, and ENSO forecasts lose predictive power. Whether these ENSO changes can be detected in the face of natural variability depends on both the magnitude of climate change and the length of the timeseries. Wind stress changes of the magnitude seen in observations over the past century, and on the order of the differences between observational analyses, appear to be just at the edge of detectability for ENSO changes in 50-year timeseries. If ENSO is as

strongly influenced by random events as the intermediate model, then interdecadal ENSO changes may be difficult to attribute to changes in the climatology. Paleodata, such as coral records and deep-ocean sediments, may be the only records long enough to cope with the significance issue and thus may prove invaluable for discerning real-world ENSO/climate relationships. Such data, of course, are beset with their own special problems: they are generally only local and indirect measures of ENSO, they may be confounded with non-ENSO effects, and it can be difficult to establish a reliable time axis for the data.

A change in the equatorial trades is also found to have a large effect on ENSO in a hybrid coupled GCM. As in the intermediate model, as the trades weaken the oscillation becomes more skewed towards cold events and shows an increased period. The HGCM is most reminiscent of the intermediate model high coupling and strengthened trades, where the intermediate model mimics the sustained variability and overly-strong cold tongue found in the HGCM. In this case the period at weak trades is strongly affected by nonlinearities, in particular the elimination of the cold tongue and equatorial upwelling during warm events, which delay the transitions from warm to cold events.

The indirect mapping between the HGCM and intermediate model underscores the importance of a broad view of ENSO, one which encompasses both its climate sensitivity and model-dependence. Well-thought-out sensitivity maps for sophisticated coupled GCMs, though expensive, would likely be invaluable tools for diagnosing problems; and similar maps for the real world (constructed from paleodata) would also be beneficial for the modeling community. Understanding these many sensitivities may well be the key to improving ENSO forecasting in the future.